Accepted Manuscript

Design, synthesis and biological evaluation of AZD9291 derivatives as selective and potent EGFR$^{L858R/T790M}$ inhibitors

Bingbing Zhao, Zhen Xiao, Jianguo Qi, Rong Luo, Zhou Lan, Yanzhuo Zhang, Xiaohan Hu, Qidong Tang, Pengwu Zheng, Shan Xu, Wufu Zhu

PII: S0223-5234(18)31028-6

DOI: https://doi.org/10.1016/j.ejmech.2018.11.069

Reference: EJMECH 10927

To appear in: *European Journal of Medicinal Chemistry*

Received Date: 26 October 2018

Revised Date: 19 November 2018

Accepted Date: 28 November 2018

Please cite this article as: B. Zhao, Z. Xiao, J. Qi, R. Luo, Z. Lan, Y. Zhang, X. Hu, Q. Tang, P. Zheng, S. Xu, W. Zhu, Design, synthesis and biological evaluation of AZD9291 derivatives as selective and potent EGFR$^{L858R/T790M}$ inhibitors, *European Journal of Medicinal Chemistry* (2019), doi: https://doi.org/10.1016/j.ejmech.2018.11.069.

Design, Synthesis and Biological Evaluation of AZD9291 Derivatives as Selective and Potent EGFR$^{L858R/T790M}$ Inhibitors

Bingbing Zhao [a], Zhen Xiao [a], Jianguo Qi [b], Rong Luo [c], Zhou Lan [a], Yanzhuo Zhang [d], Xiaohan Hu [a], Qidong Tang [a], Pengwu Zheng [a,*], Shan Xu [a,*], Wufu Zhu [a,*]

[a] Jiangxi Provincial Key Laboratory of Drug Design and Evaluation, School of Pharmacy, Jiangxi Science & Technology Normal University, 605 Fenglin Road, Nanchang, Jiangxi 330013, China

[b] Henan Provincial Key Laboratory of Natural Medicine and Immunology, Jinming Road, Kaifeng, Henan 475004, China

[c] Jiangxi Province Institute of Materia Medica, 181 East Nanjing Road, Nanchang, Jiangxi 330000, China

[d] School of Pharmacy, Xuzhou Medical University, 209 Tongshan Road, Xuzhou, Jiangsu 221004, China.

*** Corresponding author.**

Tel. & Fax: +86 791 8380-2393;

E-mail: zhengpw@126.com (P. Zheng), zhuwufu-1122@163.com (W. Zhu)

Abstract：

Third-generation epidermal growth factor receptor (EGFR)$^{L858R/T790M}$ inhibitors are still the main drugs for the treatment of advanced non-small cell lung cancer (NSCLC), and these drugs have achieved remarkable clinical efficacy. However, there are still many patients suffering from drug-resistant mutations and drug side effects caused by NSCLC. In this study, guided by the molecular simulation, we applied a structure-based drug design strategy (SBDD) and optimized the structure to obtain a series of potent and selective EGFR$^{L858R/T790M}$ inhibitors. The most potent compound **18e** demonstrated excellent kinase inhibitory activity and selectivity for EGFR$^{L858R/T790M}$ double mutants and the IC_{50} value reached nanomolar level. The selectivity of **18e** against wild-type EGFR was near to 200-fold. In addition, compound **18e** also inhibited H1975 cells proliferation at G2/M phase and induced apoptosis at a concentration of 0.25 μM, which makes it more valuable for potential lung cancer research.

Keywords: Epidermal growth factor receptor; Non-small cell lung cancer; Selectivity; L858R/T790M resistance mutation

* Corresponding author. Tel./fax: +86 791 83802393.

E-mail address: zhengpw@126.com (P. Zheng), shanxu9891@126.com (S. Xu), zhuwufu-1122@163.com (W. Zhu).

1. Introduction

Nowadays, therioma is still one of the major causes of endangering human health. Of the 7 million people that die of cancer each year, lung cancer remains the most common and deadly cancer around the world, accounting for 25% of the total number of cancer deaths [1-3]. Non-small cell lung cancer (NSCLC) is the most prevalent form of lung cancer, with approximately 1.5 million patients and a 5-year survival rate less than 20% [4,5]. Receptor tyrosine kinases (RTKs) are extensively found on cell membranes of organisms. In addition, recent studies have shown that the ErbB family plays a key role in the regulation of the physiological cycle of malignant tumors [6,7]. Epidermal growth factor receptor (EGFR) belongs to the RTKs, is considered one of the important targets for the treatment of malignant tumors, which plays a crucial role in the regulation of cancer cell growth, proliferation and differentiation [8-10].

Up to now, EGFR inhibitors have been developed to the third generation. The first-generation of EGFR inhibitors are represented by gefitinib (**1**, **Fig. 1**) and erlotinib (**2**, **Fig. 1**), They are used to treat sensitive EGFR mutations caused by the L858R mutation in exon 21 and exon 19 deletion [11,12]. In the early stage of clinical treatment, these drugs have achieved remarkable therapeutic effect. Unfortunately, more than 50% of patients treated with first-generation EGFR inhibitors developed resistance mutation (T790M) within 1 year [13]. The T790M mutation is thought to be more bulk and small-polar methionine that replaces threonine in exon 20[14]. The steric hindrance of methionine hinders the binding of drugs (gefitinib and erlotinib) to target sites in the ATP hydrophobic pocket. What's more, study have shown that the T790M mutation also increases the affinity of EGFR kinase for ATP [15,16].

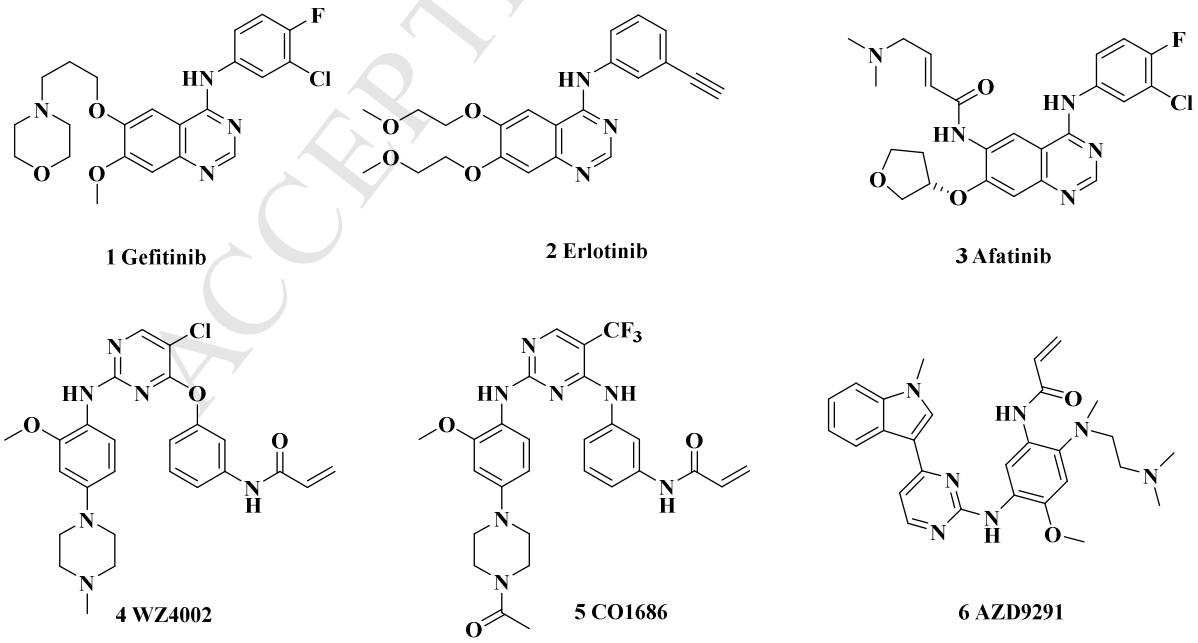

Fig. 1. Chemical structures of the representative small-molecule EGFR inhibitors.

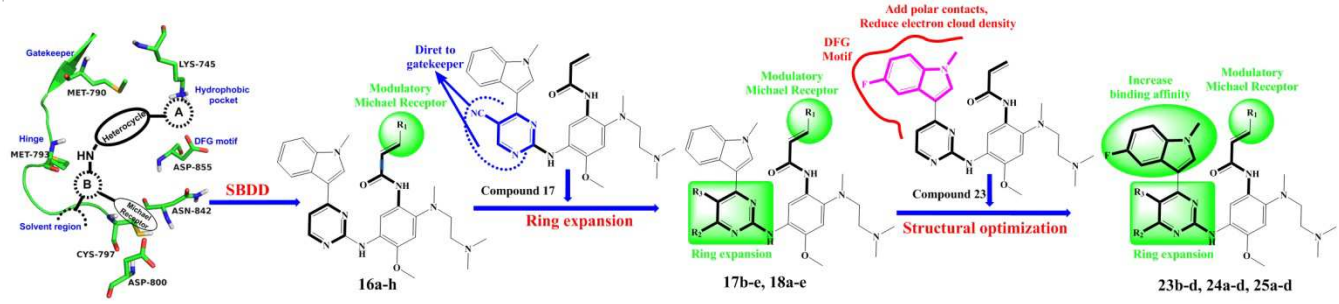

Fig. 2. Design strategy from chemical structures of previous compounds.

Consequently, many second-generation EGFR inhibitors such as afatinib (**3**, **Fig. 1**), dacomitinib and neratinib were designed for overcoming the resistance caused by T790M mutations [17-19]. Many of these medicines share the common quinazoline pharmacophore and acrylamide structure (Michael Addition Receptor). The acrylamide structure can covalently and irreversibly bind to the cysteine residue (Cys797). So, the medicine can better occupy the ATP-binding pocket of the EGFR kinase domain, and overcome the resistance caused by the T790M mutation [20]. Unexpectedly, the second-generation EGFR inhibitors not only inhibited mutational EGFR receptor but also the wild-type (WT) EGFR receptor. Therefore, most patients taking the drug within a few months experienced serious side effects such as rash, diarrhea and other side effects [21].

To overcome the drawbacks of acquired resistance to second-generation EGFR inhibitors, several third-generation EGFR inhibitors have been developed. WZ4002 (**4**, **Fig. 1**) is the first reported third-generation EGFR inhibitor and the selectivity of WZ4002 against T790M-EGFR to WT-EGFR is near to 30-100 times [22]. CO1686 (**5**, **Fig. 1**) has similar chemical structure to WZ4002, and they all share "U-shaped" molecular structure [23]. The U. S. Food and Drug Administration (FDA) was ended the Phase II clinical trial of CO1686, because it also inhibited insulin receptor (INSR) and insulin-like growth factor 1 receptor (IGF1R) causing serious side effects (especially hyperglycemia) [24]. As the first FDA-approved third-generation EGFR inhibitor, AZD9291 (**6**, **Fig. 1**) was marketed in the United States in November 2015 for treatment of $EGFR^{T790M/\ L858R}$ mutation in NSCLC patients [25]. However, the selectivity of AZD9291 to mutant kinases has not achieved the desired effect. Its binding to non-target EGFR receptors in vivo has caused serious side effects (diarrhea, rash and cardiotoxicity), which severely limits the clinical application of AZD9291. The most serious adverse event is dose-dependent toxicity, such as cardiotoxicity increased with escalating doses of AZD9291[26]. Thus, we urgently need to develop the novel EGFR inhibitors with high selectivity against WT-EGFR and low toxicity to solve the problem of drug resistance and serious side effects.

Herein, structure-based drug design (SBDD) was applied in our compounds design strategy (**Fig. 2**). Docking AZD9291 into T790M-EGFR (**Fig. 3B**) and WT-EGFR (**Fig. 3C**) revealed that the N atom in the 1-position of the pyrimidine ring points to the hinge region residue Met793, and is adjacent to the residue Met790. The acrylamide

warhead interacts with mutation gatekeeper site residue Cys797 via a hydrogen bond. The indole ring points to the Asp-Phe-Gly (DFG) motif. Furthermore, the entire binding site (**Fig. 3D**) is far away from the L858R mutant region so that the L858R mutation does not affect the binding site. Based on previous research [25,27], we first introduced small molecule substituents at the end of the acrylamide side chain to change the reactivity of the acrylamide warhead with residue Cys797. According to previous research, the two reported compounds have attracted our attention. Compound 17 was reported by Finlay, M. [26] and had good kinase inhibitory activity with an IC_{50} value of 0.9 nM for $EGFR^{T790M/L858R}$ kinase. Compound 23 was reported by Gao HY.[28], and its IC_{50} value for H1975 cells was 15 nM. Therefore, on the basis of these two compounds, we designed the next two series of compounds. The second series of compounds with different substituents at the 5-position or 6-position of the pyrimidine ring was designed by the ring expansion and splitting principle based on reported compound 17. Finally, in view of the good enzymatic and cellular inhibitory of published compound 23, we introduced fluorine into the indole ring, which presumably increases the polar interaction between the ligand and the DFG motif residue. Moreover, the F-atom can weaken the demethylation ability of the indole ring and enhances the anti-metabolism ability of AZD9291. Thus, we suspected that this design strategy may help us to discover novel inhibitors for overcoming $EGFR^{L858R/T790M}$ double mutations.

2. Results and discussion

2.1 Chemistry

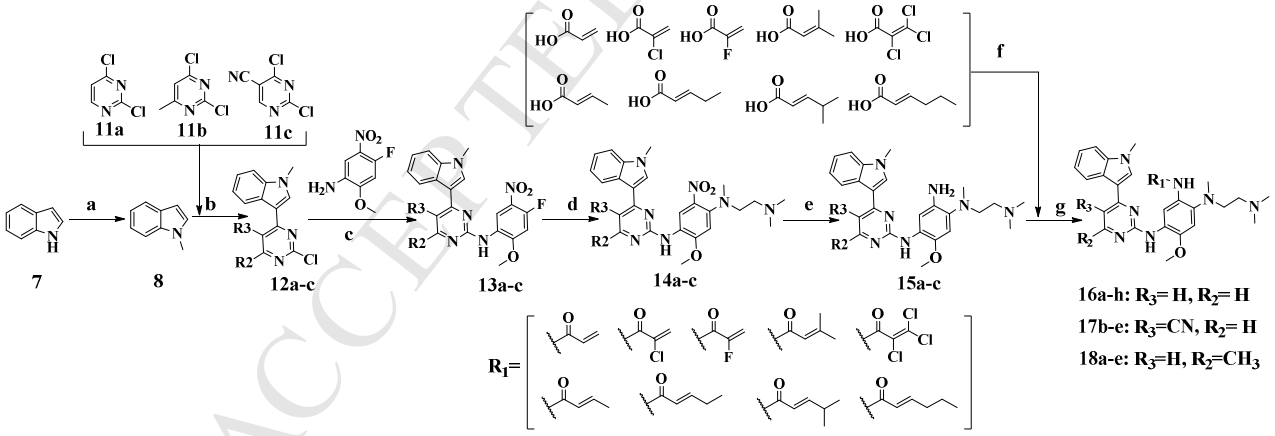

Scheme 1. Synthetic route of the compounds **16a-h**, **17b-e**, **18a-e**. Reagents and conditions: (a) CH_3I, NaH, THF, rt., 1.5 h; (b) $AlCl_3$, DME, 80 ℃, 3 h; (c) TsOH, 1,4-dioxane, 85 ℃, 3 h; (d) N,N,N-trimethylethylenediamine, DIPEA, DMA, 110 ℃, 2.5 h; (e) Zn, NH_4Cl, C_2H_5OH, H_2O, 105 ℃, 3 h; (f) $NaHCO_3$, DCM, 0 ℃, 0.5-2 h.

The synthetic route of the target compounds **16a-h**, **17b-e**, **18a-e** was shown in **Scheme 1**. Commercially available starting material indole **7** reacted with methyl iodide to get **8**. Commercially available **11a**,1**1b** and **11c** were reacted with **8** to obtain **12a-c**. Next, **12a-c** were coupled with commercially available **7** to obtain **13a-c**. **15a-c** was obtained by the reaction of amination and reduction from **14a-c** with **13a-c** as raw material. Corresponding acid chlorides were obtained

from different substituted acrylic acids by the chlorination reaction, and finally reacted with **15a-c** to provide the target compounds **16a-h**, **17b-e**, **18a-e**. The synthetic route of **23b-d**, **24a-d**, **25a-d** was outlined in **Scheme 2**, which was basically same as the route of compounds **16a-h**, **17b-e** and **18a-e**, except that the 5-fluoroindole **9** was used as the starting material. Finally, **22a-c** reacted with corresponding acid chlorides yielding compounds **23b-d**, **24a-d** and **25a-d**.

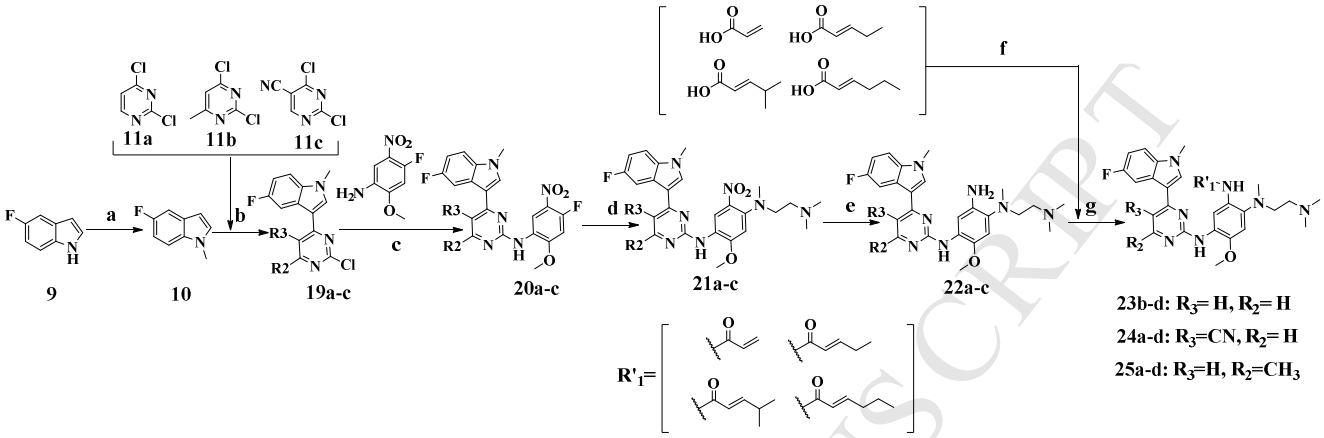

Scheme 2. Synthetic route of the compounds **23b-d**, **24a-d**, **25a-d**. Reagents and conditions: (a) CH_3I, NaH, THF, rt., 1.5 h; (b) $AlCl_3$, DME, 80 ℃, 3 h; (c) TsOH, 1,4-dioxane, 85 ℃, 3 h; (d) N,N,N'-trimethylethylenediamine, DIPEA, DMA, 110 ℃, 2.5 h; (e) Zn, NH_4Cl, C_2H_5OH, H_2O, 105 ℃, 3 h; (f) $NaHCO_3$, DCM, 0 ℃, 0.5-2 h.

2.2 Binding site analysis of AZD9291

Before conducting the experiment, we analyzed the binding site of AZD9291 with WT-EGFR (PDB code:4ZAU) and T790M-EGFR (PDB code:3IKA), respectively. The crystal complex of AZD9291 binding to WT-EGFR was available from the PDB library (http://www.rcsb.org/pdb/home/home.do). As shown in **Fig. 3C**, bidentate hydrogen bond was formed with the methionine residue Met793 between the polar hydrogen atom in the imine bridge and the N atom in the 1-position of the pyrimidine ring. In addition, cysteine residue Cys797 also formed strong hydrogen binding force with the oxygen atoms in the acrylamide side chains (bond length 2.5Å). There is no crystal complex of AZD9291 binds to T790M EGFR kinase domain in the PDB library, we simulated the binding model of published T790M structure (PDB code: 3IKA) to AZD9291 by AutoDock 4.2 software (The Scripps Research Institute, USA). From **Fig. 3 B** and **Fig. 3 D**, we can know that AZD9291 formed strong hydrogen binding force with T790M-EGFR kinase domain on the outer edge of the ATP hydrophobic pocket. Two hydrogen bonds were formed between hinge region residue Met793 (show blue in the **Fig. 3 B**) and the pyrimidine core. In addition, the L858R mutation site (show red in the **Fig. 3 B**) was far away from the small molecule ligand AZD9291 so that the firs-generation EGFR mutation would not affect the binding site. Furthermore, in our expectation, the hydrogen binding force formed between the side chain containing the Michael Addition Receptor and the Cys797 residue (show green in the **Fig. 3 B**) is stronger than that of WT-EGFR (4ZAU).

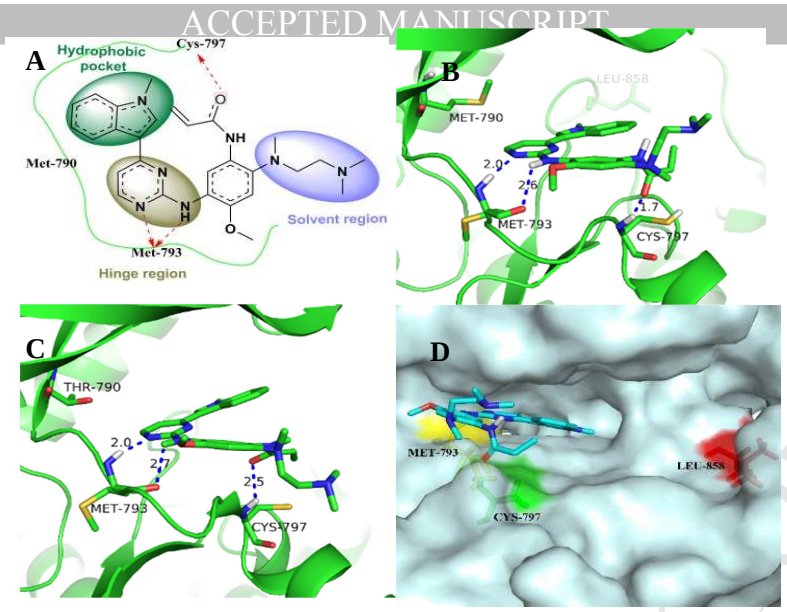

Fig. 3. Binding site of AZD9291. (A) Chemical structure of AZD9291 and its depicted binding mode with T790M-EGFR. (B) The binding model of AZD9291 (green) bound to T790M-EGFR (PDB code:3IKA). (C) The binding model of AZD9291 (green) bound to WT-EGFR (PDB code:4ZAU). (D) Overview of the binding site of AZD9291 with T790M-EGFR (PDB code:3IKA).

2.3. Modification of acrylamide side chain

It can be seen from the results of molecular simulate docking, acrylamide side chain containing Michael Addition Receptors directly extend to the Cys797 residue at the edge of the ATP hydrophobic pocket and formed stronger hydrogen binding force. Moreover, inspired by the research reported by Mark E. [27] and Xia G. [29], the introduction of small molecule alkyl side chains at the bottom of the acrylamide warhead regulates the reactivity of the olefine with residue Cys797 and impairs the irreversible binding of drug to non-targeting EGFR protein, thereby reducing the side effects of the drug. To conduct this strategy, we designed and synthesized the first series of AZD9291 derivatives with different sizes of substituents at the ortho position of the acrylamide warhead (**16a-h**) and evaluated them in enzymatic inhibition and antiproliferation activity assays.

The enzymatic and cellular activities of compounds **16a-h** were show in **Table 1**. As predicted, when we introduced strong electron withdrawing groups (-F, -Cl) into the acrylamide warhead, **16a**, **16b**, and **16c** exhibited lower antiproliferation activities against H1975 cells, and partially lost kinase activity against both $EGFR^{T790M/L858R}$ and $EGFR^{WT}$. The most gratifying result is that the kinase selectivity of all compounds against $EGFR^{T790M/L858R}$ to $EGFR^{WT}$ has been improved. The results are consistent with our expectations. We discovered compounds with high EGFR mutated kinase selectivity by modifying the structure of acrylamide. However, with the increasing of the substituted alkyl side chain, the inhibitory activity of the compounds (**16f**, **16g** and **16h**) on H1975 cells and the enzymatic inhibition against

EGFR kinase gradually increased, but it was still weaker than AZD9291. We will solve this problem in the next experiment. Accordingly, we concluded that changing the acrylamide carbon chain length csan modulate the cellular and enzymatic activity of compounds. Only when the carbon chain length of the acrylamide warhead is more than four can the cellular and enzymatic activity be improved.

Table 1

In vitro inhibitory activities of compounds **16a-h.**

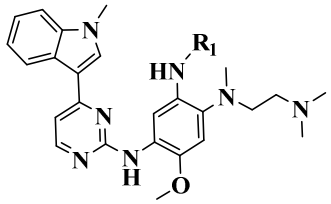

16a-h

Compd.	R^1	EGFR IC_{50} (nM)[a]		Selectivity (WT/TL)	Cellular activity IC_{50} (μM)			$LogD_{7.4}$[b]
		WT	TL		H1975	A549	HepG2	
16a		65	6	10.8	4.229	2.462	3.794	2.9
16b		257	33	7.8	1.289	7.524	1.391	3.4
16c	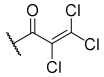	>2000	>2000	-	>50	>50	>50	4.1
16d	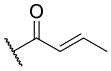	395	52	7.6	4.543	0.660	6.934	3.4
16e	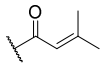	1282	209	6.1	5.606	4.096	5.663	3.6
16f	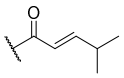	>2000	397	-	1.819	0.612	4.391	4.1
16g	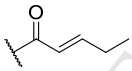	1277	177	7.2	3.862	1.533	6.674	3.8
16h	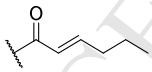	1502	203	7.4	1.219	0.808	0.431	4.2
AZD9291		16	8	2.0	0.073	0.615	1.605	3.0

[a]Enzymatic inhibitory activities assays were examined by using the ELISA-based EGFR-tyrosine kinase (TK) assay.
[b]$LogD_{7.4}$ values calculated by the chemaxon website (www.chemaxon.com).

2.4 Structure-based design of pyrimidine ring targeting Met793

From the results of our previous molecular docking (**Fig. 3 B**), we found that the pyrimidine ring of AZD9291 formed a bidentate hydrogen bond with hinge region residue Met793, with the bond lengths of 2.0Å and 2.6Å, respectively. The hydrogen bond interaction is moderate. Guided by the docking result (**Fig. 3**), we hypothesized that expanding the spatial structure of the pyrimidine ring would result in a fully occupied hinge region protein cavity. Furthermore, the -CN at the 5-position of the pyrimidine ring in compound **17** directly points to gatekeeper Met790, thus

increasing the binding capacity of protein with ligand. Consequently, based on the results of **16a-h**, we retained the alkyl-substituted acrylamide warhead and introduced small molecule substituents (-CN, -CH_3) into the pyrimidine ring to obtain compound **17b-e** and **18a-e**.

Table 2

In vitro Enzymatic inhibitory activities of compounds **17b-e** and **18a-e**.

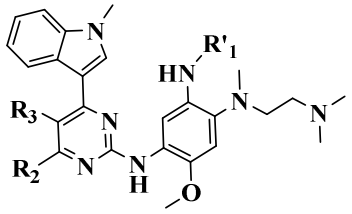

17b-e, 18a-e

Compd.	$R^{1'}$	R^2	R^3	EGFR IC_{50} (nM)[a]		Selectivity	Cellular activityIC_{50} (μM)			$LogD_{7.4}$[b]
				WT	TL	(WT/TL)	H1975	A549	HepG2	
17		-H	-CN	311	25	12.4	1.187	0.308	0.768	2.8
17b		-H	-CN	137	20	6.9	1.622	0.133	0.115	3.2
17c	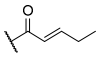	-H	-CN	387	16	24.2	1. 151	0.162	1.359	3.7
17d		-H	-CN	985	219	4.5	1.107	1.101	1.811	3.9
17e	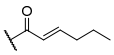	-H	-CN	377	37	10.2	0.823	0.166	1.685	4.1
18a		$-CH_3$	-H	1336	93	14.5	4.812	2.907	12.611	3.5
18b		$-CH_3$	-H	83	10	8.3	2.231	1.731	3.641	3.5
18c	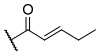	$-CH_3$	-H	1255	18	69.7	1.993	1.085	2.053	3.9
18d		$-CH_3$	-H	>2000	38	-	1.227	1.07	3.546	4.2
18e	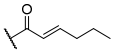	$-CH_3$	-H	1531	8	191.3	0.254	0.329	0.365	4.2
AZD9291		-H	-H	16	8	2.0	0.073	0.615	1.605	3.0

[a]Enzymatic inhibitory activities assays were examined by using the ELISA-based EGFR-tyrosine kinase (TK) assay.
[b]$LogD_{7.4}$ values calculated by the chemaxon website (www.chemaxon.com).

2.4.1 Structure-activity relationship studies of target compounds **17b-e** and **18a-e**.

The enzymatic and cellular inhibitory activities of **17b-e** and **18a-e** were shown in **Table 2**. In general, the introduction of -CN and -CH_3 into the pyrimidine ring notably increased the selectivity for WT-EGFR against double-mutant EGFR, with the selectivity from 5 to 200-fold. Moreover, the cellular anti-proliferative activity of compounds **17b-e** and **18a-e** is more potent than that of compounds **16a-h**. Particularly, compounds **18a-e,** which introduced the -CH_3 moiety, dramatically changed both the double-mutant EGFR enzymatic inhibitory activity (the IC_{50}

values from 8 to 93 nM) and the selectivity of the double-mutant EGFR against wild-type EGFR (the selectivity from 8-fold to 200-fold). We conjectured that the electron-donating group -CH_3 increased the electron cloud density of the pyrimidine ring. Hence, it enhanced the hydrogen bond reactivity between the adjacent N and the Met793 residue. We observed that **17b** was obtained by introducing a chlorine atom at the *ortho*-position of acrylamide in **17**, similar to **18a** and **18b**. However, the enzymatic activity and selectivity of both **17b** and **18b** for the double-mutant EGFR were moderately decreased; their IC_{50} values were in the range of 10 to 20 nM, and the selectivity for wild-type EGFR did not exceed 10 times. However, **17b** and **18b** also showed moderate cellular anti-proliferative activity over H1975 cells, with IC_{50} values of 1.622 μM and 2.231 μM, respectively. As the acrylamide carbon chain length increased, the enzymatic activity and selectivity underwent tremendous change. When the carbon chain length of the acrylamide warhead was 5, the IC_{50} values of **17c** and **18c** against wild-type EGFR were 387 nM and 1255 nM, respectively. When the carbon chain length was 6, the enzymatic inhibitory activity of compound **17d** and **18d** against the wild-type EGFR kinase was decreased, but the inhibitory activity against the double-mutant EGFR was retained (with IC_{50} values of 219 nM and 38 nM, respectively). Therefore, we concluded that properly increasing the acrylamide side chain length can increase the selectivity of compound to $EGFR^{T790M/L858R}$ mutant kinases and strengthen the inhibitory activity of compound to H1975 cells. In addition, by appropriately increasing the volume of pyrimidine ring, the compounds fully occupied the target protein cavity of hinge region. Therefore, it can increase the affinity of compound with target protein.

2.5 Structural modification based on the molecular simulation

2.5.1 Binding mode study of potential compounds **17c** and **18e**.

To further investigate the binding mode of compounds with EGFR, we conducted a molecular simulation of $EGFR^{T790M}$ with representative compounds **17c** and **18e** (**Fig. 4**). The binding models of compounds **17c** and **18e** with EGFR protein were the same as that of our previous hypothesis. Compound **17c** formed three hydrogen bonds with EGFR protein (The bule dashed), wherein the pyrimidine ring formed a bidentate hydrogen bond with hinge residue Met793. In addition, the -CN group at the 5-position of the pyrimidine ring directly pointed to the gatekeeper residue Met790 and adjoined the residue Thr854 with a length of 2.5Å (The red dashed). The entire conformation sufficiently occupied the protein hydrophobic cavity. The binding mode of **18e** was the same as that of **17c**. The 6-methyl-substituted pyrimidine ring was connected to the hinge residue Met793 *via* a bidentate hydrogen bond. In addition, the alkyl-substituted acrylamide side chain was adjacent to residue Cys797(with the hydrogen bond length of 2.0Å). The hydrogen binding forces of **17c** and **18e** with hinge region residue Met793 are stronger than those of AZD9291.

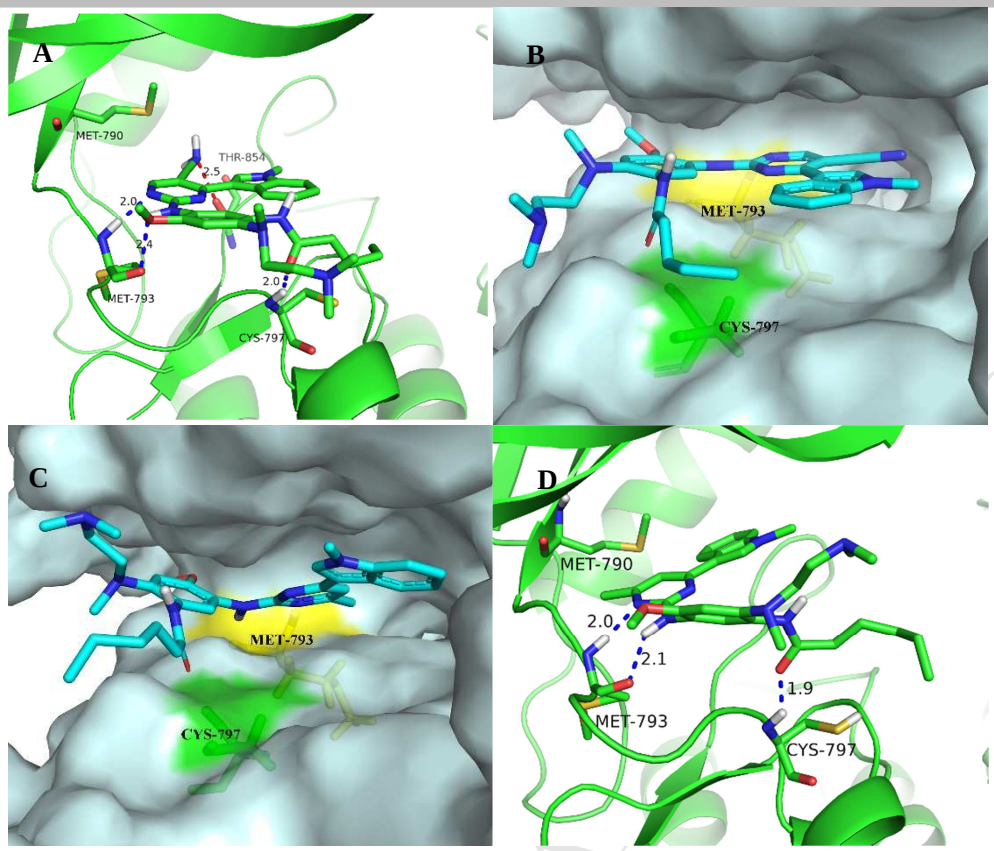

Fig. 4. Docking mode of **17c** and **18e**.

(A) Binding mode of compound **17c** bind to T790M-EGFR. (B) Overview of the binding site of compound **17c** with T790M-EGFR. (C) Overview of the binding site of compound **18e** with T790M-EGFR (D) Binding model of compound **18e** bind to T790M-EGFR.

2.5.2 Explore 5-position fluorin substitution of indole ring extend to ATP hydrophobic pocket

Since AZD9291 was approved by the FDA, many researchers are devoted to studying the in vivo metabolism and metabolites of AZD9291 to gain inspiration for the study of more potent EGFR inhibitors. Finlay MR and his co-worker were the first reported the major metabolic processes and metabolites of AZD929 in the body [26]. N-demethylation is the main metabolism way of AZD9291 in the body, produced two metabolites AZ5104 and AZ7550. Moreover, based upon the docking results of compound **17c** and **18e** with T790M active domain, indole ring burried into ATP-binding pocket and was close to DFG motif. Consequently, on the one hand, we introduced F-atom into the indole ring and amplify the volume of the indole ring to enhance the binding interaction and selectivity of the inhibitors with T790M-EGFR. On the other hand, the introduction of F-atom can weaken the demethylation ability of the indole ring and enhances the anti-metabolism ability of AZD9291c derivatives. Moreover, the strategy of introducing fluorine atom is commonly used in the development of new drugs, and compounds containing fluorine account for a significant proportion of the drugs

used for clinical treatment [30,31]. According to the metabolites of AZD9291 in vivo, Gao H. and co-workers [28] also designed and synthesized a series of derivatives of AZD9291, and conducted a detailed analysis of the results of in vivo experiments. According to their experimental results, compound **23** contained a fluorine-substituted indole ring structure exhibited $EGFR^{T790M/L858R}$ inhibitory activity.

In order to implement our design strategy, we retained $–CH_3$ and –CN on the pyrimidine ring and designed three series of fluorine-substituted derivatives at the 5-position of the indole ring (**23b-d**, **24a-d**, and **25a-d**). As shown in **Table 3**, all compounds with fluorine substituted at the 5-position of the indole ring showed obvious decreases in enzymatic activity. Accordingly, the cellular anti-proliferative activity of compounds **23b-d**, **24a-d**, and **25a-d** also moderately changed compared to compounds **17b-e**. In particular, compounds **25a-d** showed the highest decrease in both enzymatic activity and cellular activity, with IC_{50} values of H1975 cells ranging from 3.8 to 12.2 μM. On the one hand, the introduction of the strong electron-withdrawing group fluorine moiety into the indole ring that was buried in the DFG motif may greatly reduce the hydrophobic interaction between the indole and the residues of the DFG motif. On the other hand, based on the research of Gao H. [28], the introduction of fluorine reduced both the electron cloud density of the indole ring and the dealkylation ability of N-methyl indole. Thus, it can change the stability of drug structure and caused toxicity of the drug. In addition, it is also possible that the introduction of F-atom causes the compound to miss the target, and we will conduct in-depth research in future experiments. $LogD_{7.4}$ values were predicted to explain the results, and the logD7.4 values of fluorinated substitutes were 0.2 to 0.5 higher than compounds without fluorinated substitution. Most fluorinated substitutes have $logD_{7.4}$ values greater than 4.0. These results indicated that the poor solubility caused the decrease in the inhibitory activity, because the moderately lipid-soluble permeability of molecules is favorable for drugs to penetrate cell membranes.

Table 3

In vitro Enzymatic inhibitory activities of compounds **23b-d**, **24a-d** and **25a-d**

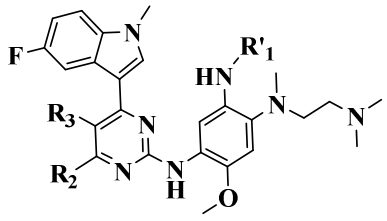

23b-d, 24a-d, 25a-d

Compd.	$R^{1'}$	R^2	R^3	EGFR IC_{50} (nM)		Selectivity	Cellular activity IC_{50} (μM)			$LogD_{7.4}$ [b]
				WT	TL	(WT/TL)	H1975	A549	HepG2	
23		-H	-H	8.7	0.07	124	0.254	0.329	0.429	3.1
23b	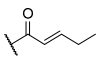	-H	-H	684	388	1.8	2.596	3.602	5.285	3.9

23c	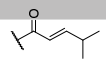	-H	-H	977	>2000	/	7.359	6.144	3.923	4.2
23d	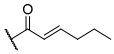	-H	-H	12	7.5	1.6	2.734	1.034	3.399	4.4
24a		-H	-CN	>2000	>2000	/	11.404	9.703	17.549	3.0
24b	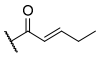	-H	-CN	>2000	>2000	/	10.209	4.725	5.881	3.8
24c		-H	-CN	415	360	1.2	1.127	0.185	2.837	4.1
24d	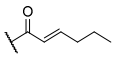	-H	-CN	1064	201	5.3	2.421	0.741	2.014	4.2
25a		$-CH_3$	-H	1094	591	1.9	3.833	1.489	4.281	3.6
25b	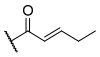	$-CH_3$	-H	>2000	998	/	10.440	9.152	10.984	4.1
25c		$-CH_3$	-H	>2000	892	/	8.520	9.083	13.998	4.4
25d	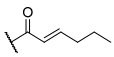	$-CH_3$	-H	>2000	923	/	12.232	13.258	12.116	4.5
AZD9291		-H	-H	16	8	2.0	0.073	0.615	1.605	3.0

[a]Enzymatic inhibitory activities assays were examined by using the ELISA-based EGFR-tyrosine kinase (TK) assay.
[b]$LogD_{7.4}$ values calculated by the chemaxon website (www.chemaxon.com).

To further investigate whether the introduction of a fluorine atom can increase the hydrogen bonding capacity, we performed molecular docking to predict the binding modes of compounds **24d** and **25b**. The docking results in Figure 5 show that compounds **24d** (**Fig. 5 A**) and **25b** (**Fig.5 B**) all formed weak hydrogen bond with the Cys797 residue (**24d** and **25b** with length of 2.3Å and 2.2Å, respectively). In addition, we can see that the -CN group of the compound **24d** lost hydrogen binding force with the residue Thr854. Neither **24d** nor **25b** engaged in hydrogen binding interactions with the residues in the DFG motif. We speculated that the F-atom is a strong electron-withdrawing group, which has a large influence on the electron cloud density of the entire molecular skeleton, and even changes the electron cloud distribution of the entire molecule. At the same time, from the LogD7.4 values, we can see that the polarity of this series of compounds does increases, which is not conducive to molecular transmembrane absorption, resulting in great changes in their activity and selectivity. We will conductced another in-depth study on F-substituted compounds.

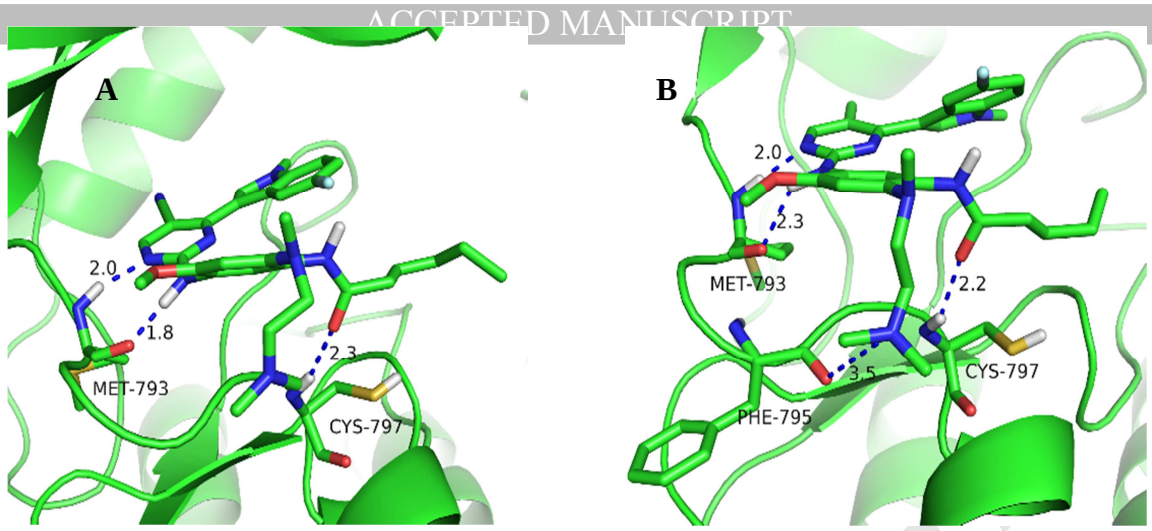

Fig. 5. Docking mode of **24d** and **25b**.

(A) The binding model of representative compounds **24d** bound to T790M-EGFR (PDB code:3IKA). (B) The binding model of representative compounds **25b** bound to T790M-EGFR (PDB code:3IKA).

2.6 Fluorescent staining is used to analyze cell morphological changes of the H1975 cells.

Fluorescence staining experiments were selected to validate and evaluate the antiproliferation by **18e** on H1975 cells. The results were shown in **Fig. 6**. AO staining fluorescence analysis results show that compared to the control group, compound **18e** significantly inhibited H1975 cells proliferation and induced apoptosis at the concentration of 0.25 μM. Moreover, after treated with compound **18e**, the chromatin of H1975 cells obviously shrink, and the cell edge were sharp. Nextly, we conducted H33342 fluorescence staining assay to further verify that compound **18e** induced H1975 cell apoptosis. As illustrated in **Fig. 6**, the control group cells structures were complete, only a small amount of dyes into cells and the nucleus showed weak blue fluorescence under inverted fluorescence microscope. While, after treatment with 0.25 μM compound **18e**, H1975 cells structures were destroyed, chromatin was shrunk, and a large amount of the dye entered cells. Hence, the dense staining was observed under an inverted fluorescence microscope and the fluorescence intensity were significantly enhanced. Those phenomenons suggested that 18e induced apoptosis. Therefore, based on the results of AO staining and H33342 staining, we can draw a conclusion that compound **18e** inhibited H1975 cell proliferation and induced apoptosis at lower concentration.

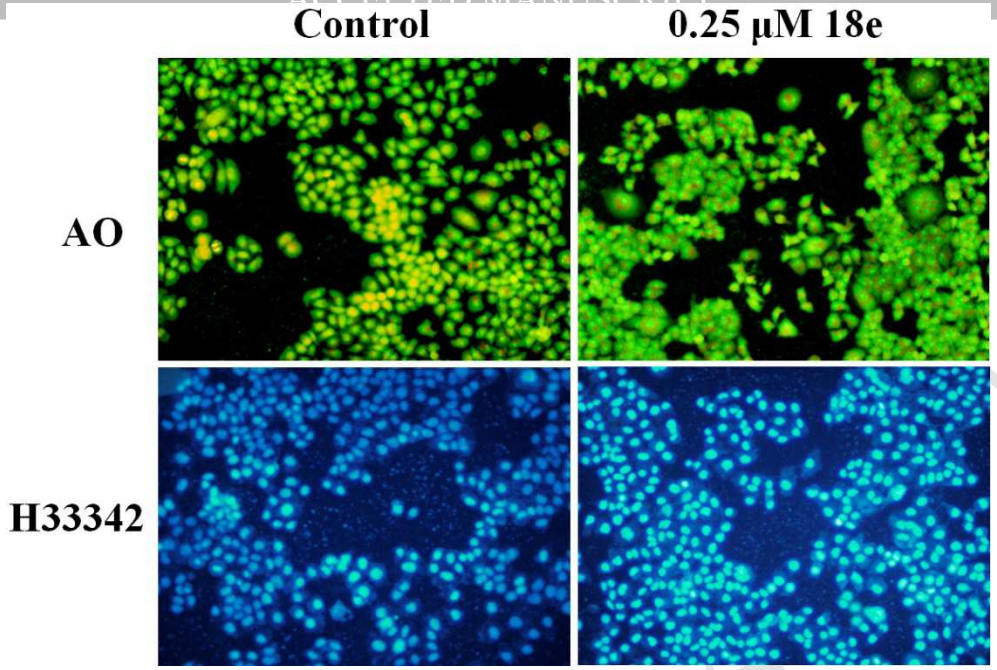

FIGURE 6. **18e** suppressed cell proliferation (acridine orange, AO) and induced apoptosis (Hoechst 33342) in H1975 cells.

2.7 Effect on cell cycle progression.

To investigate the mode of cell proliferation inhibiton by compound **18e**, cell cycle distribution analysis was performed on A549 cells. The obtained results were presented in **Fig. 7**, which shown that **18e** induced apoptosis in A549 cells at low concentration. As the concentration of compound **18e** increasing, **18e** significantly depressed the G0/G1 phase population from 56.78% to 39.55%. The number of apoptotic cells gradually increased, and the cell cycle was blocked in G2/M phase, while no significant change in S phase was observed. These findings indicated that **18e** successfully inhibited cell proliferation in a dose-dependent manner.

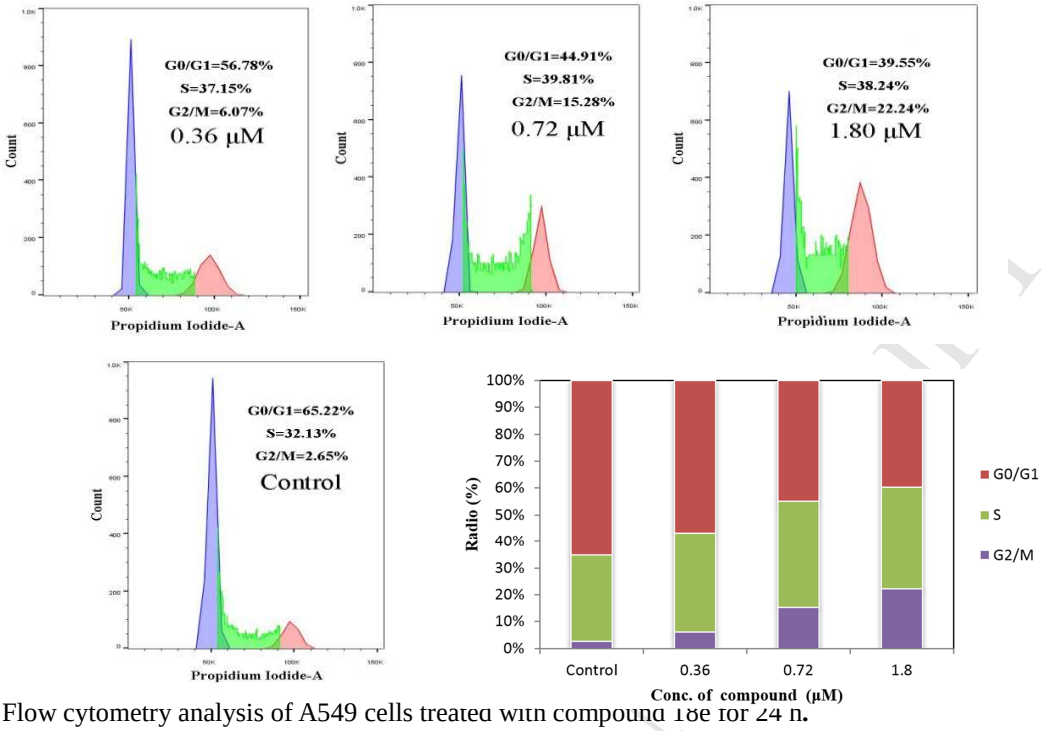

FIGURE 7. Flow cytometry analysis of A549 cells treated with compound 18e for 24 h**.**

3. Conclusions

In summary, based on potent inhibitors **17** and **23**, three series of $EGFR^{T790M/L858R}$ inhibitors were designed and synthesized. The changes in reactivity of the acrylamide warhead reduced the affinity of the medicine to non-target proteins. With the help of computer-aided drug design, we increased the spatial volume of the pyrimidine ring to enhance the selectivity of compounds for $EGFR^{T790M/L858R}$. Furthermore, based on the metabolites of AZD9291, we introduced fluorine atom into indole ring, which resulted in the compound losing its kinase selectivity. Finally, we replaced acrylamide with hexenamide and introduced methyl group at the 6-position of pyrimidine ring to obtain the optimized compound **18e** without fluorine substitution, whose physiological activity suggested that **18e** can be used as a potent $EGFRT^{790M/L858R}$ inhibitor for further study.

4. Experimental section

4.1 Chemistry

Unless otherwise required, all reagents used in the experiments were purchased from commercial analytical grade and used without further purification. Frequently used solvents (Ethanol, petroleum ether, ethyl acetate and dichloromethane, etc.) were absolutely anhydrous. All actions were monitored through GF_{254} thin-layer chromatography plate and spots were visualized with iodine or light (in 254 nm or 365 nm). The structure of the target compound was confirmed by ^{1}H NMR and ^{13}C NMR spectra at room temperature on Bruker 400 MHz spectrometer (Bruker Bioscience,

Billerica, MA, USA) with tetramethylsilane (TMS) as an internal standard. Mass spectrometry (MS) was performed on Waters High Resolution Quadrupole Time of Flight Tandem Mass Spectrometry (QTOF). The purity of the compound was determined by Agilent 1260 liquid chromatograph fitted with an Inertex-C18 column. All target compounds had purity of ≥95%.

4.1.1 General procedure for the synthesis of **16a-h**

We used indole **7** as starting material to synthesize interediates **15a-c** by the method reported in the literature [32]. Different substituted acrylic acids were chlorinated by $POCl_3$ to obtain the corresponding acyl chloride at 80 ℃. Under an ice bath, differently substituted acryl chloride was dissolved in dichloromethane and stirred at 0 ℃ for 10-30 min. Another intermediates **15a-c** were added to the above acryl chloride solution, and then added $NaHCO_3$ solid powder, stirred at 0 ℃ for 0.5-3 h. After the reaction was completed, the reaction mixture was filtered and solvent was distilled off under reduced pressure. The crude product was purified using flash chromatography with dichloromethane/methanol (v/v, from 50:1 to 20:1) as eluents.

4.1.1.1 N-(2-((2-(dimethylamino)ethyl)(methyl)amino)-4-methoxy-5-((4-(1-methyl-1H-indol-3-yl)pyrimidin-2-yl)amin amino)phenyl)-2-fluoroacrylamid (**16a**)

Light yellow solid. 37.9% yield, m.p: 190.7-192.1 ℃. ^{1}H NMR (400 MHz, DMSO-d_6) δ 10.04 (s, 1H), 8.92 (s, 1H), 8.54 (s, 1H), 8.31 (dd, J = 17.9, 6.6 Hz, 2H), 7.96 (s, 1H), 7.53 (d, J = 8.1 Hz, 1H), 7.29–7.20 (m, 2H), 7.17 (t, J = 7.4 Hz, 1H), 7.07 (s, 1H), 5.46–5.41 (m, 1H), 5.08 (d, J = 13.4 Hz, 1H), 3.91 (s, 3H), 3.89 (s, 3H), 3.27–3.22 (m, 2H), 2.87 (s, 2H), 2.65 (s, 3H), 2.58 (s, 6H); ^{13}C NMR (400 MHz, DMSO-d_6) δ 169.87, 164.85, 161.25, 158.98, 157.65, 144.25, 136.88, 134.21, 129.45, 128.96, 122.54, 122.21, 121.84, 119.98, 114.12, 111.53, 110.11, 109.86, 104.99, 99.32, 95.02, 59.23, 58.45, 56.88, 47.25×2, 42.23, 34.58. TOF MS ES+ (m/z): $(M + H)^+$, calcd for $C_{28}H_{32}FN_7O_2$: 517.2602, found, 518.2680.

4.1.1.2 2-chloro-N-(2-((2-(dimethylamino)ethyl)(methyl)amino)-4-methoxy-5-((4-(1-methyl-1H-indol-3-yl) pyrimidin -2-yl)amino)phenyl)acrylamide (**16b**)

Light yellow solid. 32.1% yield, m.p: 191.3-192.4 ℃. ^{1}H NMR (400 MHz, DMSO-d_6) δ 10.25 (s, 1H), 9.40 (s, 1H), 8.90 (s, 1H), 8.66 (t, J = 7.7 Hz, 2H), 8.33 (s, 1H), 7.86 (d, J = 8.2 Hz, 1H), 7.55 (tt, J = 15.0, 7.3 Hz, 3H), 7.37 (s, 1H), 6.22 (s, 1H), 5.99 (s, 1H), 4.23 (s, 3H), 4.19 (s, 3H), 3.23 (t, J = 4.8 Hz, 4H), 3.06 (s, 3H), 2.69 (t, J = 5.1 Hz, 2H), 2.59 (s, 6H). TOF MS ES+ (m/z): $(M + H)^+$, calcd for $C_{28}H_{32}ClN_7O_2$: 533.2306, found, 534.2384.

4.1.1.3 2,3,3-Trichloro-N-(2-((2-(dimethylamino)ethyl)(methyl)amino)-4-methoxy-5-((4-(1-methyl-1H-indol-3-yl) pyrimidin-2-yl)amino)phenyl)acrylamide (**16c**)

Light yellow solid. 36.8% yield, m.p: 287.7-288.4 ℃. ^{1}H NMR (400 MHz, DMSO-d_6) δ 11.36 (s, 1H), 9.07 (d, J =

7.3 Hz, 1H), 8.96 (s, 1H), 8.18 (s, 1H), 7.85 (d, J = 7.4 Hz, 1H), 7.56 (d, J = 8.2 Hz, 1H), 7.35 (s, 1H), 7.25 (dd, J = 15.6, 8.0 Hz, 3H), 6.92 (s, 1H), 3.90 (s, 3H), 3.67 (s, 3H), 3.20–3.02 (m, 2H), 2.89 (s, 3H), 2.26 (s, 6H). TOF MS ES+ (m/z): $(M + H)^+$, calcd for $C_{28}H_{30}C_{l3}N_7O_2$: 601.1527, found, 602.1605.

4.1.1.4 (Z)-N-(2-((2-(dimethylamino)ethyl)(methyl)amino)-4-methoxy-5-((4-(1-methyl-1H-indol-3-yl)pyrimidin-2-yl) amino)phenyl)but-2-enamide (**16d**)

White solid. 33.2% yield, m.p: 159.7-161.2 ºC. ^{1}H NMR (400 MHz, DMSO-d_6) δ 9.93 (s, 1H), 9.06 (s, 1H), 8.65 (s, 1H), 8.32 (d, J = 5.3 Hz, 1H), 8.25 (d, J = 7.9 Hz, 1H), 8.19 (s, 1H), 7.90 (s, 1H), 7.52 (d, J = 8.2 Hz, 1H), 7.23 (dd, J = 12.1, 6.3 Hz, 2H), 7.14 (t, J = 7.5 Hz, 1H), 7.02 (s, 1H), 6.81 (dq, J = 13.8, 6.9 Hz, 1H), 3.91 (s, 3H), 3.85 (s, 3H), 2.94 (d, J = 5.2 Hz, 2H), 2.69 (s, 3H), 2.46 (d, J = 5.3 Hz, 2H), 2.31 (s, 6H), 1.90 (d, J = 6.6 Hz, 3H); ^{13}C NMR (400 MHz, DMSO-d_6) δ 163.48, 162.12, 160.39, 158.12, 139.49, 138.17, 136.48, 133.29, 129.87, 128.24, 125.82, 122.46, 121.85, 121.35, 119.45, 112.91, 110.97, 108.79, 108.65, 106.42, 102.59, 59.71, 56.51, 55.87, 45.05×2, 43.12, 33.44, 18.04. TOF MS ES+ (m/z): $(M + H)^+$, calcd for $C_{29}H_{35}N_7O_2$: 513.2852, found, 514.2925.

4.1.1.5 N-(2-((2-(dimethylamino)ethyl)(methyl)amino)-4-methoxy-5-((4-(1-methyl-1H-indol-3-yl)pyrimidin-2-yl) amino)phenyl)-3-methylbut-2-enamide (**16e**)

Light yellow solid. 40.2% yield, m.p: 178.2-179.1 ºC. ^{1}H NMR (400 MHz, DMSO-d_6) δ 9.88 (s, 1H), 9.03 (s, 1H), 8.53 (s, 1H), 8.29 (t, J = 7.7 Hz, 2H), 7.96 (s, 1H), 7.49 (d, J = 8.2 Hz, 1H), 7.18 (tt, J = 15.0, 7.3 Hz, 3H), 7.00 (s, 1H), 5.85 (s, 1H), 5.62 (s, 1H), 3.86 (s, 3H), 3.82 (s, 3H), 2.86 (s, 2H), 2.69 (s, 3H), 2.32 (t, J = 5.1 Hz, 2H), 2.22 (s, 6H), 2.13 (s, 3H), 1.87 (s, 3H). TOF MS ES+ (m/z): $(M + H)^+$, calcd for $C_{30}H_{37}N_7O_2$: 527.3009, found, 528.3087.

4.1.1.6 (Z)-N-(2-((2-(dimethylamino)ethyl)(methyl)amino)-4-methoxy-5-((4-(1-methyl-1H-indol-3-yl)pyrimidin-2-yl) amino)phenyl)-4-methylpent-2-enamide (**16f**)

White solid. 35.7% yield, m.p: 208.2-209.6 ºC. ^{1}H NMR (400 MHz, DMSO-d_6) δ 10.04 (s, 1H), 9.13 (s, 1H), 8.67 (s, 1H), 8.32 (d, J = 5.2 Hz, 1H), 8.23 (d, J = 7.8 Hz, 1H), 7.92 (d, J = 24.3 Hz, 1H), 7.53 (d, J = 8.1 Hz, 1H), 7.23 (t, J = 6.5 Hz, 2H), 7.15 (t, J = 7.4 Hz, 1H), 7.02 (s, 1H), 6.80 (d, J = 6.5 Hz, 1H), 6.09 (d, J = 14.9 Hz, 1H), 3.91 (s, 3H), 3.85 (s, 3H), 2.89 (s, 2H), 2.71 (d, J = 9.7 Hz, 3H), 2.41 (dd, J = 17.0, 10.3 Hz, 3H), 2.26 (s, 6H), 1.07 (d, J = 6.7 Hz, 5H); ^{13}C NMR (400 MHz, DMSO-d_6) δ 168.74, 166.08, 159.98, 157.21, 151.27, 142.89, 136.24, 134.05, 129.87, 128.45, 123.21, 122.23, 121.98, 120.87, 119.82, 113.52, 111.25, 109.87, 109.42, 104.71, 98.87, 59.78, 56.82, 55.49, 46.02x2, 42.08, 33.89, 25.09, 20.92×2. TOF MS ES+ (m/z): $(M + H)^+$, calcd for $C_{31}H_{39}N_7O_2$: 541.3165, found, 542.3242.

4.1.1.7 (Z)-N-(2-((2-(dimethylamino)ethyl)(methyl)amino)-4-methoxy-5-((4-(1-methyl-1H-indol-3-yl)pyrimidin-2-yl) amino)phenyl)pent-2-enamide (**16g**)

Light yellow solid. 37.4% yield, m.p: 245.6-247.1 ºC. ^{1}H NMR (400 MHz, DMSO-d_6) δ 10.72 (s, 1H), 9.73 (s, 1H),

8.70 (s, 1H), 8.26 (s, 2H), 7.54 (s, 1H), 7.36–7.14 (m, 4H), 7.03–6.75 (m, 3H), 3.91 (s, 3H), 3.85 (s, 3H), 2.73 (s, 6H), 2.62 (s, 3H), 2.20 (s, 2H), 1.35–1.20 (m, 4H), 1.04 (s, 3H). TOF MS ES+ (m/z): $(M + H)^+$, calcd for $C_{30}H_{37}N_7O_2$: 527.3009, found, 528.3087.

4.1.1.8 (Z)-N-(2-((2-(dimethylamino)ethyl)(methyl)amino)-4-methoxy-5-((4-(1-methyl-1H-indol-3-yl)pyrimidin-2-yl) amino)phenyl)hex-2-enamide (**16h**)

White solid. 34.1% yield, m.p: 185.2-186.7 ºC. ^{1}H NMR (400 MHz, DMSO-d_6) δ 10.02 (s, 1H), 9.13 (s, 1H), 8.68 (s, 1H), 8.32 (d, J = 5.3 Hz, 1H), 8.24 (d, J = 7.8 Hz, 1H), 7.90 (s, 1H), 7.53 (d, J = 8.2 Hz, 1H), 7.24 (t, J = 6.7 Hz, 2H), 7.15 (t, J = 7.4 Hz, 1H), 7.03 (s, 1H), 6.81 (dtd, J = 11.0, 6.9, 3.8 Hz, 2H), 6.11 (d, J = 15.3 Hz, 1H), 5.80–5.72 (m, 1H), 3.92 (s, 3H), 3.85 (s, 3H), 2.90 (s, 2H), 2.71 (s, 3H), 2.36 (s, 2H), 2.24 (d, J = 7.5 Hz, 6H), 2.14 (dd, J = 13.7, 6.5 Hz, 2H), 1.50–1.42 (m, 2H), 0.93 (dd, J = 13.5, 6.2 Hz, 3H); ^{13}C NMR (400 MHz, DMSO-d_6) δ 167.72, 163.33, 160.35, 158.17, 148.83, 146.23, 144.00, 138.18, 134.35, 128.31, 125.90, 125.81, 125.77, 122.78, 122.42, 121.78, 121.35, 112.94, 110.97, 107.59, 105.68, 57.16, 56.50, 55.89, 45.51×2, 43.01, 33.83, 21.66, 21.30, 13.96. TOF MS ES+ (m/z): $(M + H)^+$, calcd for $C_{31}H_{39}N_7O_2$: 541.3165, found, 543.3245.

4.1.2 General procedure for the synthesis of **17b-e**

The synthetic method of compounds **17b-e** are similarly to **16a-h**. The difference is that we need to replace the pyrimidine with cyan-substituted pyrimidine and the rest of the synthesis conditions are the same.

4.1.2.1 2-chloro-N-(5-((5-cyano-4-(1-methyl-1H-indol-3-yl)pyrimidin-2-yl)amino)-2-((2-(dimethylamino)ethyl) (methyl)amino)-4-methoxyphenyl)acrylamide (**17b**)

Pure white solid. 38.9% yield, m.p: 152.3-153.1 ºC. ^{1}H NMR (400 MHz, DMSO-d_6) δ 10.03 (s, 1H), 9.45 (s, 1H), 8.69 (s, 1H), 8.50 (s, 1H), 8.24 (s, 1H), 7.53 (d, J = 7.6 Hz, 1H), 7.33–7.20 (m, 1H), 7.14 (s, 1H), 6.47 (s, 1H), 6.29 (s, 1H), 6.07 (s, 1H), 5.86 (s, 1H), 3.92 (s, 3H), 3.78 (s, 3H), 3.26–3.19 (m, 2H), 2.76 (s, 2H), 2.72 (s, 3H), 2.47 (s, 6H); ^{13}C NMR (400 MHz, DMSO-d_6) δ 173.87, 165.21, 164.87, 163.52, 143.78, 137.85, 136.53, 133.89, 130.08, 129.32, 123.54, 122.32, 121.38, 121.05, 119.87, 113.92, 113.27, 111.23, 109.88, 109.26, 98.53, 96.73, 59.81, 58.08, 55.78, 46.18×2, 41.25, 35.09. TOF MS ES+ (m/z): $(M + H)^+$, calcd for $C_{29}H_{31}ClN_8O_2$: 558.2259, found, 559.2337.

4.1.2.2 (Z)-N-(5-((5-cyano-4-(1-methyl-1H-indol-3-yl)pyrimidin-2-yl)amino)-2-((2-(dimethylamino)ethyl)(methyl) amino)-4-methoxyphenyl)pent-2-enamide (**17c**)

Pure white solid. 44.1% yield, m.p: 128.5-130.1 ºC. ^{1}H NMR (400 MHz, DMSO-d_6) δ 9.92 (s, 1H), 9.41 (d, J = 9.0 Hz, 1H), 8.67 (s, 1H), 8.48 (s, 1H), 8.38 (s, 1H), 7.51 (d, J = 7.5 Hz, 1H), 7.23 (s, 1H), 7.06 (s, 1H), 6.91–6.73 (m, 2H), 6.05 (d, J = 15.4 Hz, 1H), 5.74 (d, J = 15.6 Hz, 1H), 3.91 (s, 3H), 3.72 (s, 3H), 2.91 (s, 2H), 2.74 (d, J = 10.9 Hz, 3H), 2.39 (s, 2H), 2.23 (d, J = 5.8 Hz, 6H), 2.20–2.14 (m, 2H), 1.02 (dd, J = 9.8, 7.5 Hz, 3H). TOF MS ES+ (m/z): $(M + H)^+$,

calcd for $C_{31}H_{36}N_8O_2$:552.6830, found, 553.3048.

4.1.2.3 (Z)-N-(5-((5-cyano-4-(1-methyl-1H-indol-3-yl)pyrimidin-2-yl)amino)-2-((2-(dimethylamino)ethyl)(methyl) amino)-4-methoxyphenyl)-4-methylpent-2-enamide (**17d**)

Pure white solid. 41.2% yield, m.p: 160.3-162.1 ºC. ^{1}H NMR (400 MHz, $CDCl_3$) δ 9.35 (s, 1H), 9.26 (s, 1H), 8.65 (s, 1H), 8.49 (s, 2H), 7.78 (s, 1H), 7.36 (d, J = 7.3 Hz, 1H), 7.33–7.27 (m, 2H), 6.92 (d, J = 16.8 Hz, 2H), 6.72 (s, 1H), 3.91 (d, J = 6.6 Hz, 6H), 3.29 (s, 2H), 3.01 (s, 2H), 2.74 (d, J = 11.2 Hz, 9H), 2.53 (d, J = 6.8 Hz, 1H), 1.10 (d, J = 6.8 Hz, 6H); ^{13}C NMR (400 MHz, DMSO-d_6) δ 174.31, 166.25, 164.28, 162.87, 151.82, 142.98, 136.58, 133.52, 129.85, 128.32, 122.53, 121.38, 121.07, 119.88, 119.05, 114.08, 113.87, 111.84, 109.86, 109.43, 98.72, 96.02, 59.87, 57.98, 57.03, 47.86×2, 41.05, 34.08, 24.87, 22.23×2. TOF MS ES+ (m/z): $(M + H)^+$, calcd for $C_{32}H_{38}N_8O_2$: 566.3118, found, 567.3203 .

4.1.2.4 (Z)-N-(5-((5-cyano-4-(1-methyl-1H-indol-3-yl)pyrimidin-2-yl)amino)-2-((2-(dimethylamino)ethyl) (methyl) amino)-4-methoxyphenyl)hex-2-enamide (**17e**)

Pure white solid. 39.1% yield, m.p: 158.1-160.6 ºC. ^{1}H NMR (400 MHz, DMSO-d_6) δ 9.92 (s, 1H), 9.40 (s, 1H), 8.66 (s, 1H), 8.47 (s, 1H), 8.37 (s, 1H), 7.51 (d, J = 8.2 Hz, 1H), 7.23 (s, 1H), 7.05 (s, 1H), 6.82–6.69 (m, 2H), 6.07 (d, J = 15.3 Hz, 1H), 5.75 (d, J = 15.5 Hz, 1H), 3.90 (s, 3H), 3.72 (s, 3H), 2.91 (s, 2H), 2.74 (s, 3H), 2.41 (d, J = 5.8 Hz, 2H), 2.23 (s, 6H), 2.17–2.13 (m, 2H), 1.45–1.41 (m, 2H), 0.89–0.87 (m, 3H). TOF MS ES+ (m/z): $(M + H)^+$, calcd for $C_{32}H_{38}N_8O_2$: 556.3118, found, 567.3192.

4.1.3 General procedure for the synthesis of **18a-e.**

The synthetic method of compounds **18a-e** are similarly to **16a-h**. The difference is that we need to replace the pyrimidine with methyl-substituted pyrimidine and the rest of the synthesis conditions are the same.

4.1.3.1 N-(2-((2-(dimethylamino)ethyl)(methyl)amino)-4-methoxy-5-((4-methyl-6-(1-methyl-1H-indol-3-yl) pyrimidin -2-yl) amino)phenyl)acrylamide (**18a**)

Light yellow solid. 31.9% yield, m.p: 292.7-293.4 ºC. ^{1}H NMR (400 MHz, DMSO-d_6) δ 10.90 (s, 1H), 9.89 (s, 1H), 9.05 (s, 1H), 8.64 (s, 1H), 8.22 (s, 1H), 7.52 (d, J = 7.0 Hz, 1H), 7.35 (d, J = 10.9 Hz, 1H), 7.27–7.14 (m, 3H), 6.95 (s, 1H), 6.24 (d, J = 18.6 Hz, 1H), 5.68 (d, J = 10.2 Hz, 1H), 3.90 (d, J = 3.3 Hz, 3H), 3.89 (s, 3H), 3.29 (s, 3H), 3.15 (s, 2H), 2.73 (s, 6H), 2.59 (s, 2H), 2.49 (s, 3H). TOF MS ES+ (m/z): $(M + H)^+$, calcd for $C_{29}H_{35}N_7O_2$:513.2852, found, 514.2931.

4.1.3.2 2-chloro-N-(2-((2-(dimethylamino)ethyl)(methyl)amino)-4-methoxy-5-((4-methyl-6-(1-methyl-1H-indol-3-yl) pyrimidin-2-yl)amino)phenyl)acrylamide (**18b**)

Light yellow solid. 31.5% yield, m.p: 164.5-165.7 ºC. ^{1}H NMR (400 MHz, DMSO-d_6) δ 9.94 (s, 1H), 9.12 (s, 1H),

8.53 (s, 1H), 8.16 (d, J = 8.0 Hz, 1H), 7.69 (s, 1H), 7.43 (d, J = 8.1 Hz, 1H), 7.15 (t, J = 7.6 Hz, 1H), 7.09 (t, J = 7.8 Hz, 2H), 6.99 (s, 1H), 6.49 (d, J = 2.1 Hz, 1H), 6.03 (d, J = 2.1 Hz, 1H), 3.83 (s, 3H), 3.81 (s, 3H), 3.18 (t, J = 7.0 Hz, 2H), 2.82 (t, 2H), 2.57 (s, 3H), 2.40 (s, 6H), 2.29 (s, 3H). TOF MS ES+ (m/z): $(M + H)^+$, calcd for $C_{29}H_{34}ClN_7O_2$: 547.2463, found, 548.2544.

4.1.3.3 (Z)-N-(2-((2-(dimethylamino)ethyl)(methyl)amino)-4-methoxy-5-((4-methyl-6-(1-methyl-1H-indol-3-yl) pyrimidin-2-yl)amino)phenyl)pent-2-enamide (**18c**)

Light yellow solid. 34.4% yield, m.p: 189.7-191.2 ºC. ^{1}H NMR (400 MHz, DMSO-d_6) δ 9.83 (s, 1H), 9.15 (s, 1H), 8.57 (s, 1H), 8.03 (d, J = 8.0 Hz, 1H), 7.54 (s, 1H), 7.33 (d, J = 8.1 Hz, 1H), 7.09–7.01 (m, 1H), 6.97 (t, J = 7.2, 5.5 Hz, 2H), 6.82 (s, 1H), 6.69 (ddt, J = 21.8, 15.5, 6.3 Hz, 2H), 3.73 (s, 3H), 3.67 (s, 3H), 2.70 (t, 2H), 2.36–2.28 (m, 3H), 2.19 (s, 3H), 2.16 (t, J = 6.2 Hz, 2H), 2.06 (s, 6H), 2.01–1.95 (m, 2H), 0.88 (t, J = 7.4 Hz, 3H); ^{13}C NMR (400 MHz, DMSO-d_6) δ 168.72, 168.06, 165.84, 160.89, 145.03, 142.56, 136.52, 133.24, 129.55, 128.31, 123.08, 121.85, 120.63, 119.51, 119.75, 113.82, 111.21, 109.58, 109.01, 104.53, 98.27, 58.86, 58.32, 56.81, 47.23×2, 41.45, 33.87, 25.24, 19.85, 14.68. TOF MS ES+ (m/z): $(M + H)^+$, calcd for $C_{31}H_{39}N_7O_2$: 576.2854, found, 577.2935.

4.1.3.4 (Z)-N-(2-((2-(dimethylamino)ethyl)(methyl)amino)-4-methoxy-5-((4-methyl-6-(1-methyl-1H-indol-3-yl) pyrimidin-2-yl)amino)phenyl)-4-methylpent-2-enamide (**18d**)

Light yellow solid. 38.2% yield, m.p: 172.3-173.5 ºC. ^{1}H NMR (400 MHz, DMSO-d_6) δ 9.86 (s, 1H), 9.20 (s, 1H), 8.58 (s, 1H), 8.03 (d, J = 8.0 Hz, 1H), 7.53 (s, 1H), 7.33 (d, J = 8.2 Hz, 1H), 7.04 (t, J = 7.7 Hz, 1H), 6.98 (d, J = 4.6 Hz, 2H), 6.82 (s, 1H), 6.63 (ddd, J = 6.5, 15.5, 30.9 Hz, 2H), 3.74 (s, 3H), 3.68 (s, 3H), 2.69 (t, J = 5.7 Hz, 2H), 2.34 (t, J = 11.4, 13.2 Hz, 3H), 2.17 (d, J = 22.2 Hz, 6H), 2.06 (s, 6H), 0.89 (d, J = 6.7 Hz, 6H). TOF MS ES+ (m/z): $(M + H)^+$, calcd for $C_{32}H_{41}N_7O_2$: 555.3322, found, 556.3405.

4.1.3.5 (Z)-N-(2-((2-(dimethylamino)ethyl)(methyl)amino)-4-methoxy-5-((4-methyl-6-(1-methyl-1H-indol-3-yl) pyrimidin-2-yl)amino)phenyl)hex-2-enamide (**18e**)

Light yellow solid. 39.4% yield, m.p: 129.4-131.1 ºC. ^{1}H NMR (400 MHz, DMSO-d_6) δ 9.80 (s, 1H), 9.15 (s, 1H), 8.57 (s, 1H), 8.04 (d, J = 8.0 Hz, 1H), 7.54 (s, 1H), 7.33 (d, J = 8.1 Hz, 1H), 7.04 (t, J = 7.4 Hz, 1H), 7.00–6.94 (m, 2H), 6.83 (s, 1H), 6.66–6.56 (m, 2H), 3.74 (s, 3H), 3.68 (s, 3H), 2.72 (t, J = 5.7 Hz, 2H), 2.31 (t, J = 1.9 Hz, 3H), 2.20 (d, J = 4.5 Hz, 5H), 2.09 (s, 6H), 2.05–2.01 (m, 2H), 1.31 (q, J = 7.4 Hz, 2H), 0.75 (t, J = 7.4 Hz, 3H); ^{13}C NMR (400 MHz, DMSO-d_6) δ 167.89, 166.97, 165.84, 160.25, 143.84, 139.54, 136.25, 133.34, 129.28, 128.65, 122.87, 122.23, 120.87, 120.08, 119.25, 113.87, 111.08, 109.87, 109.23, 104.87, 98.27, 59.21, 57.53, 55.82, 46.25×2, 41.87, 34.08, 28.27, 24.32, 21.89, 16.78. TOF MS ES+ (m/z): $(M + H)^+$, calcd for $C_{32}H_{41}N_7O_2$: 555.3322, found, 556.3400.

4.1.4 General procedure for the synthesis of **23b-d**

The synthetic method of compounds **23b-d** are similarly to **16a-h**. The difference is that we need to replace the indole with fluorine-substituted indole and the rest of the synthesis conditions are the same.

4.1.1.1 (Z)-N-(2-((2-(dimethylamino)ethyl)(methyl)amino)-5-((4-(5-fluoro-1-methyl-1H-indol-3-yl)pyrimidin-2-yl) amino)-4-methoxyphenyl)pent-2-enamide (**23b**)

White solid. 35.1% yield, m.p: 194.6-195.7 ºC. ^{1}H NMR (400 MHz, DMSO-d_6) δ 9.87 (s, 1H), 8.71 (s, 1H), 8.61 (s, 1H), 8.29 (d, J = 4.7 Hz, 1H), 8.05 (d, 1H), 7.54 (s, 1H), 7.23 (d, J = 5.7 Hz, 1H), 7.09 (d, J = 7.4 Hz, 3H), 6.58 (s, 1H), 6.09 (s, 1H), 3.91–3.87 (m, 7H), 3.18–3.13 (m, 2H), 2.73 (s, 9H), 2.66 (s, 2H); ^{13}C NMR (400 MHz, DMSO-d_6) δ 170.82, 166.45, 160.21, 157.01, 156.87, 144.89, 143.21, 133.77, 132.12, 129.88, 128.96, 122.53, 122.31, 115.03, 113.26, 112.87, 112.43, 111.12, 108.98, 104.53, 98.23, 58.67, 56.78, 55.96, 47.18×2, 41.25, 33.68, 20.05, 13.89. TOF MS ES+ (m/z): $(M + H)^+$, calcd for $C_{30}H_{36}FN_7O_2$: 545.2915, found, 546.2995.

4.1.4.2 (Z)-N-(2-((2-(dimethylamino)ethyl)(methyl)amino)-5-((4-(5-fluoro-1-methyl-1H-indol-3-yl)pyrimidin-2-yl) amino)-4-methoxyphenyl)-4-methylpent-2-enamide (**23c**)

White solid. 34.3% yield, m.p: 123.7-125.1 ºC. ^{1}H NMR (400 MHz, DMSO-d_6) δ 9.83 (s, 1H), 8.57 (s, 1H), 8.03 (d, J = 8.0 Hz, 1H), 7.54 (s, 1H), 7.33 (d, J = 8.1 Hz, 1H), 7.07–7.01 (m, 1H), 6.97 (q, J = 7.2, 5.5 Hz, 3H), 6.82 (s, 1H), 6.68 (tt, J = 15.5, 6.5 Hz, 2H), 3.73 (s, 3H), 3.67 (s, 3H), 2.73–2.68 (m, 2H), 2.35–2.29 (m, 3H), 2.15 (s, 2H), 2.06 (s, 6H), 2.01–1.95 (m, 2H), 0.80 (t, J = 7.4 Hz, 3H). TOF MS ES+ (m/z): $(M + H)^+$, calcd for $C_{31}H_{38}FN_7O_2$:559.3071, found, 560.3161.

4.1.4.3 (Z)-N-(2-((2-(dimethylamino)ethyl)(methyl)amino)-5-((4-(5-fluoro-1-methyl-1H-indol-3-yl)pyrimidin-2-yl) amino)-4-methoxyphenyl)hex-2-enamide (**23d**)

White solid. 36.2% yield, m.p: 211.9-213.4 ºC. ^{1}H NMR (400 MHz, DMSO-d_6) δ 9.93 (s, 1H), 8.92 (s, 1H), 8.62 (s, 1H), 8.28 (d, J = 5.3 Hz, 1H), 8.09 (s, 1H), 8.02 (d, J = 10.7 Hz, 1H), 7.53 (dd, J = 9.0, 4.5 Hz, 1H), 7.17 (d, J = 5.3 Hz, 1H), 7.12–7.04 (m, 1H), 7.01 (s, 1H), 6.78 (dd, J = 15.5, 6.1 Hz, 1H), 6.11 (d, J = 15.4 Hz, 1H), 2.95 (s, 2H), 2.69 (s, 3H), 2.53 (s, 3H), 2.35 (s, 6H), 1.07 (s, 3H), 1.05 (s, 3H); ^{13}C NMR (400 MHz, DMSO-d_6) δ 169.71, 166.58, 159.83, 157.98, 157.56, 143.96, 139.84, 133.54, 132.02, 130.25, 128.87, 122.53,122.05, 114.93, 113.81, 112.59, 112.31, 111.23, 109.25, 104.36, 98.63, 59.27, 58.63, 56.87, 48.03×2, 40.82, 34.25, 28.76, 22.56, 15.28. TOF MS ES+ (m/z): $(M + H)^+$, calcd for $C_{31}H_{38}FN_7O_2$:559.3071, found, 560.3150.

4.1.5 General procedure for the synthesis of **24a-d**

The synthetic method of compounds **24a-d** are similarly to **16a-h**. The difference is that we need to replace the indole and pyrimidine with fluorine-substituted indole and cyan-substituted pyrimidine, respectively. The rest of the synthesis conditions are the same.

4.1.5.1 N-(5-((5-cyano-4-(5-fluoro-1-methyl-1H-indol-3-yl)pyrimidin-2-yl)amino)-2-((2-(dimethylamino)ethyl)(methyl)amino)-4-methoxyphenyl)acrylamide (**24a**)

White solid. 39.3% yield, m.p: 155.8-159.3 ºC. ^{1}H NMR (400 MHz, DMSO-d_6) δ 10.70 (s, 1H), 9.97 (s, 1H), 8.78 (s, 1H), 8.25 (s, 2H), 7.58 (d, J = 8.0 Hz, 1H), 7.37 (d, J = 6.6 Hz, 1H), 7.27 (d, J = 6.3 Hz, 2H), 7.01 (s, 1H), 6.20 (d, J = 17.0 Hz, 1H), 5.69 (d, J = 10.3 Hz, 1H), 3.92 (s, 3H), 3.85 (s, 3H), 3.34 (s, 2H), 2.75 (s, 3H), 2.64 (s, 2H), 2.50 (s, 6H). TOF MS ES+ (m/z): $(M + H)^+$, calcd for $C_{29}H_{31}FN_8O_2$: 542.2554, found, 543.2632.

4.1.5.2 (Z)-N-(5-((5-cyano-4-(5-fluoro-1-methyl-1H-indol-3-yl)pyrimidin-2-yl)amino)-2-((2-(dimethylamino)ethyl)(methyl)amino)-4-methoxyphenyl)pent-2-enamide (**24b**)

White solid. 40.8% yield, m.p: 135.1-136.7 ºC. ^{1}H NMR (400 MHz, DMSO-d_6) δ 9.66 (s, 1H), 9.42 (s, 1H), 8.51 (s, 1H), 8.35 (s, 1H), 8.05 (s, 1H), 7.35 (s, 1H), 6.94 (s, 2H), 6.32 (s, 1H), 6.09 (s, 1H), 5.87 (s, 1H), 3.72 (s, 3H), 3.63 (s, 3H), 3.19 (t, J = 7.0 Hz, 2H), 2.88 (t, J = 7.3 Hz, 2H), 2.54 (d, J = 14.9 Hz, 3H), 2.50 (s, 6H), 2.33 (s, 2H), 1.02 (t, J = 9.3 Hz, 3H); ^{13}C NMR (400 MHz, DMSO-d_6) δ 164.40, 163.70, 162.53, 161.39, 158.87, 151.59, 141.98, 137.07, 135.81, 134.14, 133.23, 123.40, 122.12, 120.36, 119.71, 112.12, 112.02, 111.62, 111.36, 111.05, 106.33, 101.98, 56.37, 54.66, 50.43, 43.82, 43.08×2, 34.14, 29.47, 14.37. TOF MS ES+ (m/z): $(M + H)^+$, calcd for $C_{31}H_{35}FN_8O_2$: 570.2867, found, 571.2950.

4.1.5.3 (Z)-N-(5-((5-cyano-4-(5-fluoro-1-methyl-1H-indol-3-yl)pyrimidin-2-yl)amino)-2-((2-(dimethylamino)ethyl)(methyl)amino)-4-methoxyphenyl)-4-methylpent-2-enamide (**24c**)

White solid. 44.1% yield, m.p: 179.8-181.2 ºC. ^{1}H NMR (400 MHz, DMSO-d_6) δ 9.66 (s, 1H), 9.42 (s, 1H), 8.51 (s, 1H), 8.35 (s, 1H), 8.05 (s, 1H), 7.35 (s, 1H), 6.94 (s, 2H), 6.32 (s, 1H), 6.09 (s, 1H), 5.87 (s, 1H), 5.62 (s, 1H), 3.72 (s, 3H), 3.63 (s, 3H), 3.19 (d, J = 7.1 Hz, 2H), 2.88 (d, J = 7.2 Hz, 2H), 2.52 (s, 3H), 2.50 (s, 6H), 2.33 (s, 2H), 1.01 (s, 3H); ^{13}C NMR (400 MHz, DMSO-d_6) δ 164.23, 163.75, 162.64, 161.66, 155.15, 150.80, 142.55, 135.85, 134.26, 127.12, 123.03, 122.84, 120.95, 120.02, 119.90, 112.21, 112.11, 111.72, 111.45, 111.23, 109.05, 106.29, 56.30, 55.82, 44.39, 42.56, 34.25, 30.63, 29.58, 22.02×2, 21.67. TOF MS ES+ (m/z): $(M + H)^+$, calcd for $C_{32}H_{37}FN_8O_2$: 584.3204, found, 585.3102.

4.1.5.4 (Z)-N-(5-((5-cyano-4-(5-fluoro-1-methyl-1H-indol-3-yl)pyrimidin-2-yl)amino)-2-((2-(dimethylamino)ethyl)(methyl)amino)-4-methoxyphenyl)hex-2-enamide (**24d**)

White solid. 43.2% yield, m.p: 141.7-142.5 ºC. ^{1}H NMR (400 MHz, DMSO-d_6) δ 9.71 (s, 1H), 9.57 (s, 1H), 8.66 (s, 1H), 8.53 (s, 1H), 8.25 (s, 1H), 7.53 (s, 1H), 7.05 (d, J = 25.2 Hz, 2H), 6.75 (ddd, J = 31.4, 15.5, 6.3 Hz, 2H), 6.34 (d, J = 15.9 Hz, 1H), 3.90 (s, 3H), 3.74 (s, 3H), 3.10 (s, 2H), 2.86 (s, 2H), 2.68 (s, 3H), 2.50 (s, 6H), 2.44–2.40 (m, 1H), 1.20 (s, 6H); ^{13}C NMR (400 MHz, DMSO-d_6) δ 163.75, 163.19, 162.02, 160.98, 159.63, 157.29, 150.86, 144.29, 142.14, 135.28,

133.67, 126.59, 126.48, 124.70, 122.55, 119.26, 111.69, 111.60, 111.14, 110.88, 110.53, 105.56, 66.28, 55.76, 54.25, 42.84, 42.44, 33.68, 33.38, 28.96, 21.08, 13.55. TOF MS ES+ (m/z): $(M + H)^+$, calcd for $C_{32}H_{37}FN_8O_2$: 584.3204, found, 585.3107.

4.1.6 General procedure for the synthesis of **25a-d**

The synthetic methods of compound **25a-d** are similarly to **16a-h**. The difference is that we need to replace the indole and pyrimidine with fluorine-substituted indole and methyl-substituted pyrimidine, respectively. The rest of the synthesis conditions are the same.

4.1.6.1 N-(2-((2-(dimethylamino)ethyl)(methyl)amino)-5-((4-(5-fluoro-1-methyl-1H-indol-3-yl)-6-methylpyrimidin-2-yl)amino)-4-methoxyphenyl)acrylamide (**25a**)

Light yellow solid. 50.3% yield, m.p: 245.1-246.3 ºC. ^{1}H NMR (400 MHz, DMSO-d_6) δ 9.32 (s, 1H), 8.73 (s, 1H), 7.86 (s, 1H), 7.50–7.43 (m, 2H), 7.42 (s, 1H), 7.35 (dd, J = 7.5, 4.9 Hz, 1H), 7.03 (td, J = 7.8, 1.5 Hz, 1H), 6.38 (s, 1H), 6.31 (t, J = 13.4 Hz, 1H), 5.90 (dd, J = 13.6, 3.1 Hz, 1H), 5.83 (dd, J = 13.4, 3.1 Hz, 1H), 3.84 (s, 3H), 3.77 (s, 3H), 3.69 (t, J = 7.1 Hz, 2H), 3.00 (s, 3H), 2.74 (t, J = 7.1 Hz, 2H), 2.42 (s, 3H), 2.33 (s, 6H); ^{13}C NMR (400 MHz, DMSO-d_6) δ 170.02, 169.32, 168.72, 162.03, 158.4, 144.21, 134.65, 132.52, 131.45, 131.23, 129.87, 126.98, 122.83, 115.54, 113.98, 112.98, 112.65, 111.53, 110.23, 104.97, 98.98, 58.96, 57.25, 56.38, 45.85×2, 42.08, 34.85, 25.35. TOF MS ES+ (m/z): $(M + H)^+$, calcd for $C_{29}H_{34}FN_7O_2$: 531.2758, found, 532.2836.

4.1.6.2 (Z)-N-(2-((2-(dimethylamino)ethyl)(methyl)amino)-5-((4-(5-fluoro-1-methyl-1H-indol-3-yl)-6-methylpyrimidin-2-yl)amino)-4-methoxyphenyl)pent-2-enamide (**25b**)

Light yellow solid. 52.5% yield, m.p: 239.7-240.1 ºC. ^{1}H NMR (400 MHz, DMSO-d_6) δ 9.24 (s, 1H), 8.73 (s, 1H), 7.86 (s, 1H), 7.51–7.40 (m, 3H), 7.34 (dd, J = 7.5, 4.9 Hz, 1H), 7.04 (td, J = 7.7, 1.5 Hz, 1H), 6.38 (s, 1H), 6.22–6.15 (m, 2H), 3.84 (s, 3H), 3.77 (s, 3H), 3.69 (t, J = 7.1 Hz, 2H), 3.00 (s, 3H), 2.74 (t, J = 7.1 Hz, 2H), 2.45–2.36 (m, 5H), 2.33 (s, 6H), 1.08(m, 3H). TOF MS ES+ (m/z): $(M + H)^+$, calcd for $C_{31}H_{38}FN_7O_2$:559.3071, found, 560.3145.

4.1.6.3 (Z)-N-(2-((2-(dimethylamino)ethyl)(methyl)amino)-5-((4-(5-fluoro-1-methyl-1H-indol-3-yl)-6-methylpyrimidin-2-yl)amino)-4-methoxyphenyl)-4-methylpent-2-enamide (**25c**)

Light yellow solid. 46.3% yield, m.p: 208.5-209.4 ºC. ^{1}H NMR (400 MHz, DMSO-d_6) δ 9.35 (s, 1H), 8.70 (s, 1H), 7.86 (s, 1H), 7.52 (s, 1H), 7.48 (m, 2H), 7.35 (dd, J = 7.5, 5.0 Hz, 1H), 7.04 (td, J = 7.8, 1.5 Hz, 1H), 6.38 (s, 1H), 6.22 (dd, J = 11.0, 0.9 Hz, 1H), 6.02 (m, 1H), 3.84 (s, 3H), 3.77 (s, 3H), 3.69 (t, J = 7.1 Hz, 2H), 3.00 (s, 3H), 2.74 (t, J = 7.1 Hz, 2H), 2.66 (m, 1H), 2.42 (s, 3H), 2.34 (s, 6H), 1.04 (dd, J = 6.8, 1.1 Hz, 6H); ^{13}C NMR (400 MHz, DMSO-d_6) δ 170.21, 169.53, 167.24, 161.56, 157.98, 151.93, 143.99, 133.98, 132.57, 130.81, 129.39, 122.86, 119.84, 115.53, 113.88, 112.98, 112.57, 111.53, 109.88, 105.23, 99.02, 59.23, 57.69, 56.89, 46.92×2, 42.12, 35.08, 24.98, 24.32, 22.46×2. TOF

MS ES+ (m/z): $(M + H)^+$, calcd for $C_{32}H_{40}FN_7O_2$: 573.3228, found, 574.3306.

4.1.6.4 (Z)-N-(2-((2-(dimethylamino)ethyl)(methyl)amino)-5-((4-(5-fluoro-1-methyl-1H-indol-3-yl)-6-methylpyrimidin-2-yl)amino)-4-methoxyphenyl)hex-2-enamide (**25d**)

Light yellow solid. 58.7% yield, m.p: 195.7-196.6 ºC. ^{1}H NMR (400 MHz, DMSO-d_6) δ 9.21 (s, 1H), 8.70 (s, 1H), 7.86 (s, 1H), 7.52 (s, 1H), 7.48 – 7.40 (m, 2H), 7.35 (dd, J = 7.5, 5.0 Hz, 1H), 7.04 (td, J = 7.8, 1.5 Hz, 1H), 6.38 (s, 1H), 6.28 (dt, J = 10.8, 6.1 Hz, 1H), 6.20–6.14 (m, 1H), 3.84 (s, 3H), 3.77 (s, 3H), 3.69 (t, J = 7.1 Hz, 2H), 3.00 (s, 3H), 2.74 (t, J = 7.1 Hz, 2H), 2.42 (s, 3H), 2.35–2.27 (m, 8H), 1.49 (m, 2H), 0.89 (t, J = 8.0 Hz, 3H). TOF MS ES+ (m/z): $(M + H)^+$, calcd for $C_{32}H_{40}FN_7O_2$: 573.3228, found, 574.3312.

4.2 Molecular docking study

All the molecular docking simulation were carried out by the AutoDock 4.2 software (The Scripps Research Institute, USA). The docking tutorial we used and the detailed AutoDock basic operation methods can be found at: http://autodock.scripps.edu/faqs-help/tutorial. The protein preparation process of flexible docking mainly includes fixing the exact residues, adding hydrogen atoms, removing irrelevant water molecules and adding charges, etc. The crystal structure (PDB: 4ZAU, http://www.pdb.org/) of WT-EGFR bind to inhibitor **6** and the crystal structure (PDB: 3IKA, http://www.pdb.org/) of T790M-EGFR bind to inhibitor **4** were used in the docking studies. We first removed inhibitors **4** and **6** from their crystal structure, then put target compounds in the binding site. Finally, we used genetic algorithm to optimize energy. Only the best-scoring ligand-protein complexe was used for the binding site analysis. All the docking results were processed and modified in PyMOL 1.8.x software (https://pymol.org).

4.3 In vitro enzymatic activity assay

All compounds we designed and synthesized were tested for their activity against $EGFR^{WT}$ and $EGFR^{T790M/L858R}$ by mobility shift assay with ATP concentration at Km. Compounds were diluted with 100% DMSO to require maximum inhibitory concentration, and then transfer 100 μL of the compound dilution to a well in a 96-well plate. For all compounds, they were tested from 1μM, 3-fold dilution for 5 points. The kinase reaction contained 0.04 ng/μL $EGFR^{WT}$ or 0.02 ng/μL $EGFR^{T790M/L858R}$, 0.5 μM substrate-biotin, 10 μM ATP, 1 mM DTT, 1 mM $MnCl_2$ and 5 mM $MgCl_2$. Kinase react and stop incubate at 28℃ for specified period of time. Add 25 μL stop buffer to stop reaction, then collect data on Caliper and copy conversion data from Caliper program. Percent inhibition = (max-conversion)/(max-min) ×100.“max” stands for DMSO control; “min” stands for low control.

4.4 In vitro anti-proliferative activity assay

H1975, HepG2 and A549 cell were obtained from the Cell Cultures Collection of Chinese Academy of Sciences (Shanghai Institutes for Biological Sciences, Chinese Academy of Sciences). We tested the anti-proliferative effect of all

compounds against above cancer cell lines by the standard MTT assay in vitro, with EGFR inhibitor AZD9291 as positive control. All cells were maintained and propagated as monolayer at 37 ºC for 24 h in 5% CO_2 incubator in DMEM or RPMI1640 containing 10% fetalbovine serum. A certain concentration of test compounds were added to the culture medium for further 72 hours and fresh MTT reagent (Thiazolyl blue tetrazolium bromide) was added to each well at a concentration of 5 μg/mL and incubated with cells for 4 hours at 37 ºC. The formazan crystals were dissolved in 100 μL DMSO each well. The absorbency at 492 nm (for absorbance of MTT formazan) and 630 nm (for the reference wavelength) was measured with the ELISA reader. All of compounds were tested three times in each of cell lines. The results expressed as inhibition rates or IC_{50} (half-maximal inhibitory concentration) were the averages of two determinations and calculated by using the Bacus Laboratories Incorporated Slide Scanner (Bliss) software.

4.5 Cell cycle progression assay

A549 cells were seeded in a 6-well plate at 1×10^5 cells per well and incubated for 24 h. Then cells were treated with vehicle (0.1% DMSO) or different concentrations of **18e** for 24 h. Cells were harvested and fixed with ice-cold 70% ethanol at 4ºC for 12 h. Ethanol was removed and the cells were washed with cold PBS. Then cells were incubated in 0.5 mL of PBS containing 1 mg/mL Rnase for 30 min at 37ºC. Then the cells were stained with propidium iodide (PI) in the dark for 30 min. The DNA contents was then measured by flow cytometer.

5. Acknowledgements

We gratefully acknowledge the generous support provided by The National Natural Science Funds of China (No. 21662014), Jiangxi Outstanding Youth Talent Support Program (20171BCB23078), Natural Science Foundation of Jiangxi, China (20171ACB21052, 20181BBG70003, 20181ACB20025), Jiangxi Science and Technology Normal University Innovative Research Team (2017CXTD002).

6. References

1. Song Z, Ge Y, Wang C, *et al*. Challenges and perspectives on the development of small-molecule EGFR inhibitors against T790M-mediated resistance in non-small-cell lung cancer[*J*]. *Journal of Medicinal Chemistry*, 2016,59(14):6580-6594
2. Gschwind A, Fischer OM, Ullrich A. *et al*. The discovery of receptor tyrosine kinases: targets for cancer therapy[*J*]. *Nature Reviews Cancer*, 2004, 4(5):361-370.
3. Chico L K, Van Eldik L J, Watterson D M. *et al*. Targeting protein kinases in central nervous system disorders[*J*]. *Nature Reviews Drug Discovery*, 2009, 8(11):892-909.
4. Torre L A, Bray F, Siegel R L, *et al*. Global cancer statistics, 2012[*J*]. *Ca A Cancer Journal for Clinicians*, 2015, 65(2):87-108.

5. Ciardiello F, Tortora G. A Novel Approach in the Treatment of Cancer: Targeting the Epidermal Growth Factor Receptor[*J*]. *Clinical Cancer Research*, 2001, 7(10):2958-2970.
6. Olayioye M A, Neve R M, Lane H A, *et al*. The ErbB signaling network: receptor heterodimerization in development and cancer[*J*]. *Embo Journal*, 2000, 19(13):3159-3167.
7. Hynes N E, Lane H A. ERBB receptors and cancer: the complexity of targeted inhibitors[*J*]. *Nature Reviews Cancer*, 2005, 5(5):341-354.
8. Tiseo M, Bartolotti M, Gelsomino F, *et al*. Emerging role of gefitinib in the treatment of non-small-cell lung cancer (NSCLC)[*J*]. *Drug Design Development & Therapy*, 2010, 4(1):81-98.
9. Ren Y, Yao Y, Ma Q, *et al*. EGFR gene-mutation status correlated with therapeutic decision making in lung adenocarcinoma[*J*]. *Oncotargets & Therapy*, 2015, 8:3017-3020.
10. Zhang Q, Wang Z, Guo J, *et al*. Comparison of single-agent chemotherapy and targeted therapy to first-line treatment in patients aged 80 years and older with advanced non-small-cell lung cancer[*J*]. *Oncotargets & Therapy*, 2015, 8:893-898.
11. Shepherd F A, Rodrigues P J, Ciuleanu T, *et al*. Erlotinib in previously treated non-small-cell lung cancer[*J*]. *New England Journal of Medicine*, 2005, 353(2):123-132.
12. Maemondo M, Inoue A, Kobayashi K, *et al*. Gefitinib or chemotherapy for non–small-cell lung cancer with mutated EGFR[*J*]. *New England Journal of Medicine*, 2010, 362(25):2380-2388.
13. Kobayashi S, Boggon TJ, Dayaram T, *et al*. Mutation and resistance of non–small-cell lung cancer to gefitinib[*J*]. *New England Journal of Medicine*, 2005, 352(8):786-792
14. Yamane H, Ochi N, Yasugi M, *et al*. Docetaxel for non-small-cell lung cancer harboring the activated EGFR mutation with T790M at initial presentation[*J*]. *Oncotargets & Therapy*, 2013, 6(1):155-160.
15. Yun CH, Mengwasser KE, Toms AV, *et al*. The T790M mutation in EGFR kinase causes drug resistance by increasing the affinity for ATP[*J*]. *Proceedings of the National Academy of Sciences of the United States of America*, 2008, 105(6):2070-2075.
16. Pawar V G, Sos M L, Rode H B, *et al*. Synthesis and biological evaluation of 4-anilinoquinolines as potent inhibitors of epidermal growth factor receptor[*J*]. *Journal of Medicinal Chemistry*, 2010, 53(7):2892-2901.
17. Solca F, Dahl G, Zoephel A, *et al*. Target binding properties and cellular activity of afatinib (BIBW 2992), an irreversible ErbB family blocker[*J*]. *Journal of Pharmacology & Experimental Therapeutics*, 2012, 343(2):342-350.
18. Jänne P A, Ou S H, Kim D W, *et al*. Dacomitinib as first-line treatment in patients with clinically or molecularly selected advanced non-small-cell lung cancer: a multicentre, open-label, phase 2 trial[*J*]. *Lancet Oncology*, 2014, 15(13):1433-1441.

19. Bose P, Ozer H. Neratinib: an oral, irreversible dual EGFR/HER2 inhibitor for breast and non-small cell lung cancer[*J*]. *Expert Opinion Investigational Drugs*, 2009, 18(11):1735-1751.

20. Liu Q, Sabnis Y, Zhao Z, *et al*. Developing irreversible inhibitors of the protein kinase cysteinome[*J*]. *Chemistry & Biology*, 2013, 20(2):146-159.

21. Sos M L, Rode H B, Heynck S, *et al.* Chemogenomic profiling provides insights into the limited activity of irreversible EGFR Inhibitors in tumor cells expressing the T790M EGFR resistance mutation[*J*]. *Cancer Research*, 2010, 70(3):868-874.

22. Zhou W, Ercan D, Chen L, *et al.* Novel mutant-selective EGFR kinase inhibitors against EGFR T790M.[*J*]. *Nature*, 2009, 462(7276):1070-1074.

23. Walter AO, Sjin RT, Haringsma HJ, *et al*. Discovery of a mutant-selective covalent inhibitor of EGFR that overcomes T790M-mediated resistance in NSCLC[*J*]. *Cancer discovery*, 2013, 3(12):1404-1415.

24. Tomassi S, Lategahn J, Engel J, *et al.* Indazole-based covalent inhibitors to target drug resistant epidermal growth factor receptor[*J*]. *Journal of Medicinal Chemistry*, 2017, 60(6):2361-2372.

25. Cross D A, Ashton S E, Ghiorghiu S, *et al*. AZD9291, an irreversible EGFR TKI, overcomes T790M-mediated resistance to EGFR inhibitors in lung cancer[*J*]. *Cancer Discovery*, 2014, 4(9):1046-1061.

26. Finlay M R, Anderton M, Ashton S, *et al*. Discovery of a potent and selective EGFR inhibitor (AZD9291) of both sensitizing and T790M resistance mutations that spares the wild type form of the receptor[*J*]. *Journal of Medicinal Chemistry*, 2014, 57(20):8249-8267.

27. Flanagan M E, Abramite J A, Anderson D P, *et al*. Chemical and computational methods for the characterization of covalent reactive groups for the prospective design of irreversible inhibitors[*J*]. *Journal of Medicinal Chemistry*, 2014, 57(23):10072-10079.

28. Gao H, Yang Z, Yang X, *et al*. Synthesis and evaluation of osimertinib derivatives as potent EGFR inhibitors[*J*]. *Bioorganic Medicinal Chemistry*, 2017, 25(17):4553-4559.

29. Xia G, Chen W, Zhang J, *et al*. A chemical tuned strategy to develop novel irreversible EGFR-TK inhibitors with improved safety and pharmacokinetic profiles[*J*]. *Journal of Medicinal Chemistry*, 2014, 57(23):9889-9900.

30. Hagmann W K. The many roles for fluorine in medicinal chemistry[*J*]. *Journal of Medicinal Chemistry*, 2008, 51(15):4359-69.

31. Ojima, Iwao. Use of Fluorine in the Medicinal Chemistry and Chemical Biology of Bioactive Compounds-A Case Study on Fluorinated Taxane Anticancer Agents[*J*]. *Chembiochem*, 2004, 5(5):628-635.

32. Astrazeneca AB, Astrazeneca UL. 2-(2,4,5-Substituted anilino) pyrimidine derivatives as EGFR modulators useful for treating cancer Marie Patent: WO2013/14448 A1, 2013, 50–161.

Table of Contents

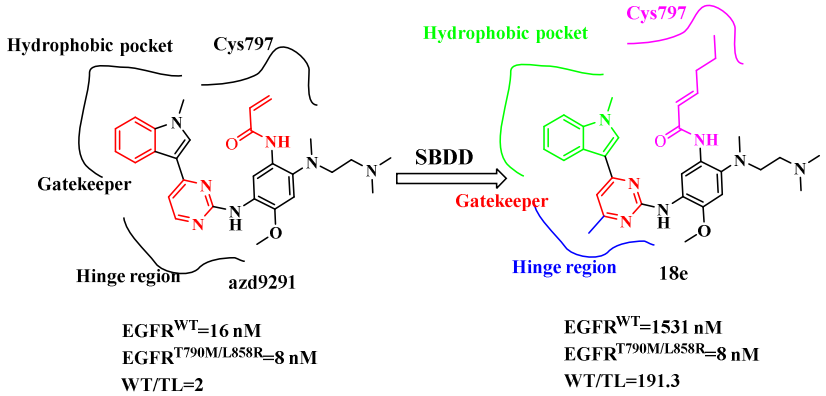

$EGFR^{WT}$=16 nM
$EGFR^{T790M/L858R}$=8 nM
WT/TL=2

$EGFR^{WT}$=1531 nM
$EGFR^{T790M/L858R}$=8 nM
WT/TL=191.3

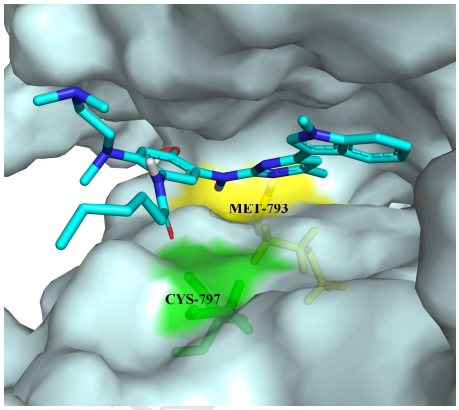

Based on the structure-activity relationship of AZD9291, three series of AZ9291 derivatives bearing Pyrimidine phenyl acrylamide structure were designed, synthesized. Moreover, antitumour activity, enzyme-based selectivity, AO staining, H33342 staining, cell cycle progression and docking study were carried out.

Research Highlights

- Three series of potent and selective $EGFR^{L858R/T790M}$ inhibitors were designed and characterized.
- Most of the synthesized compounds showed moderate to significant antitumor activity.
- The selectivity of **18e** against wild-type EGFR was near to 200-fold. **18e** arrest efficiently the cell cycle progression in G2/ M phase of A549 cells.
- Docking study was investigated to explore the binding modes of compounds with $EGFR^{T790M}$.